

**STUDIES OF P3HT:PCBM THIN FILM FORMATION
FOR POLYMER SOLAR CELLS**

MOHD NIZAM BIN YUSLI

**DISSERTATION SUBMITTED IN FULFILMENT OF
THE REQUIREMENTS FOR THE DEGREE
OF MASTER OF SCIENCE**

**DEPARTMENT OF PHYSICS
FACULTY OF SCIENCE
UNIVERSITY OF MALAYA
KUALA LUMPUR**

2013

UNIVERSITI MALAYA

ORIGINAL LITERARY WORK DECLARATION

Name of Candidate: **Mohd Nizam Bin Yusli** (I.C/Passport No:**840205-08-6123**)

Registration/Matric No: **SGR070039**

Name of Degree: **Master of Science (Dissertation)**

Title of Project Paper/Research Report/Dissertation/Thesis ("this Work"):
STUDIES OF P3HT:PCBM THIN FILM FORMATION FOR POLYMER SOLAR CELLS

Field of Study: **Organic Electronic**

I do solemnly and sincerely declare that:

- (1) I am the sole author/writer of this Work;
- (2) This Work is original;
- (3) Any use of any work in which copyright exists was done by way of fair dealing and for permitted purposes and any excerpt or extract from, or reference to or reproduction of any copyright work has been disclosed expressly and sufficiently and the title of the Work and its authorship have been acknowledged in this Work;
- (4) I do not have any actual knowledge nor do I ought reasonably to know that the making of this work constitutes an infringement of any copyright work;
- (5) I hereby assign all and every rights in the copyright to this Work to the University of Malaya ("UM"), who henceforth shall be owner of the copyright in this Work and that any reproduction or use in any form or by any means whatsoever is prohibited without the written consent of UM having been first had and obtained;
- (6) I am fully aware that if in the course of making this Work I have infringed any copyright whether intentionally or otherwise, I may be subject to legal action or any other action as may be determined by UM.

Candidate's Signature

Date

Mohd Nizam Bin Yusli

Subscribed and solemnly declared before,

Witness's Signature

Date

Name: **Dr. Khaulah Sulaiman**
Designation: **Senior Lecturer**

ABSTRACT

Bulk heterojunction polymer solar cell is widely investigated throughout the decade. This is due to its potential as an alternative to inorganic solar cell such as silicon-base solar cell. Compared to inorganic solar cell, polymer solar cell is low in cost, much easier to fabricate and shows higher mechanical flexibility. Two types of conjugated polymers has been used in this study; [6,6]-phenyl-C61-butyric acid methyl ester (PCBM) and poly(3-hexylthiophene) (P3HT). Many methods have been used to improve the efficiency of the solar cell. Thermal treatment on the organic layers has been utilized to increase the solar cell efficiency by improving the morphology and structure of the sample. It has been reported that by using different preparation methods, such as 'slow grown' and 'fast grown', the efficiency is enhanced. The morphology of the sample also varies when different solvent are used. In this study, we report the effect of thermal treatment on the optical, structural and morphological properties of the P3HT:PCBM blend thin films. The absorption, Raman, photoluminescence as well as x-ray diffraction spectra of the films will be discussed. The influence of thermal treatment on the performance of the P3HT:PCBM-based solar cells also investigated.

The effect of solvent used also been discuss in this study. The polymer materials solutions were prepared using two types of solvents; 100% dichlorobenzene (DCB), 100% chloroform and 50%:50% mixture of DCB and chloroform. Then, the morphological characterizations of P3HT:PCBM bulk thin films were carried out by UV-Visible absorption spectroscopy, X-ray diffraction (XRD) spectroscopy, Atomic Force Microscopy (AFM) and Scanning electron microscopy (SEM). Furthermore, the P3HT:PCBM photoactive layer was sandwiched between two different electrodes of

aluminum (Al) and indium tin oxide (ITO) to form the polymeric-based solar cells, namely ITO/P3HT:PCBM/Al devices.

In this study it has been found that the thermal treatment process has a significant effect on the sample. Using different fabrication process also play a major role in improving the structure of the sample. Other than that, results of this study also indicate that solar cells employing the P3HT:PCBM bulk thin films prepared from the solvent mixture exhibit the enhanced fill factor and short-circuit current than that of other cells.

ABSTRAK

Sel solar polimer *bulk heterojunction* telah dikaji dengan meluas sepanjang dekad ini. Ini adalah disebabkan potensinya sebagai alternatif kepada sel solar bukan organik seperti sel solar yang berasaskan silikon. Berbanding sel solar bukan organik, sel solar polimer adalah berkos rendah, lebih mudah untuk dihasilkan dan menunjukkan fleksibiliti mekanikal yang lebih tinggi. Dua jenis polimer konjugat yang digunakan dalam kajian ini; [6,6]-phenyl-C61-butyric acid methyl ester (PCBM) and poly(3-hexylthiophene) (P3HT). Banyak kaedah telah digunakan untuk meningkatkan kecekapan sel solar. Rawatan terma pada lapisan organik telah digunakan untuk meningkatkan kecekapan sel solar dengan meningkatkan morfologi dan struktur sampel. Juga telah dilaporkan sebelum ini, bahawa dengan menggunakan kaedah penyediaan yang berbeza, seperti ‘penumbuhan perlahan’ dan ‘penumbuhan cepat’, kecekapan sel solar dapat dipertingkatkan. Morfologi sampel juga didapati berbeza apabila menggunakan pelarut yang berbeza. Dalam kajian ini, kesan rawatan haba pada ciri-ciri optik, struktur dan morfologi campuran filem nipis P3HT:PCBM telah dilaporkan. Spektra keserapan, Raman, fotoluminesen dan juga penyerakan Sinar-X akan dibincangkan. Pengaruh rawatan terma pada prestasi sel solar berasaskan P3HT:PCBM juga disiasat.

Kesan pelarut yang digunakan juga dibincangkan dalam kajian ini. Larutan bahan polimer telah disediakan dengan menggunakan dua jenis pelarut; 100% diklorobenzena (DCB), 100% kloroform dan 50%:50% campuran DCB dan kloroform. Pencirian morfologi filem nipis P3HT:PCBM telah dijalankan menggunakan Spektroskopi serapan UV-cahaya nampak, Spektroskopi Penyerakan Sinar-X, Mikroskopi Daya Atom (AFM) dan Mikroskopi Imbasan Elektron (SEM). Selain daripada itu, lapisan aktif-foto P3HT:PCBM diapit di antara dua elektrod aluminium

(Al) dan Indium tin oksida (ITO) untuk membentuk sel-sel solar berasaskan polimer, iaitu peranti ITO/P3HT:PCBM/Al.

Dalam kajian ini telah ditemui bahawa proses rawatan terma mempunyai kesan yang besar ke atas sampel. Menggunakan proses fabrikasi yang berbeza juga memainkan peranan besar dalam meningkatkan struktur sampel. Selain daripada itu, hasil kajian ini juga menunjukkan bahawa sel-sel solar yang menggunakan filem nipis P3HT:PCBM yang disediakan daripada campuran pelarut mempamerkan peningkatan 'fill factor' dan arus litar-pintas berbanding sel-sel yang lain.

Acknowledgements

First and foremost I want to thank my Supervisor Dr Khaulah Sulaiman. It has been an honor to be her first master student. She has taught me, guided me both consciously and un-consciously. I appreciate all her contributions of time, ideas, and funding to make my master degree experience productive and stimulating. The enthusiasm she has for her research was contagious and motivational for me, even during tough times in the master degree pursuit. I am also thankful for her patients she has shown me throughout these long years during my process of finishing my master degree. The members of the Solid State Laboratory group have contributed immensely to my personal and professional time at University of Malaya. The group has been a source of friendships as well as good advice and collaboration. To be honest, I already consider them to be my brothers and sisters. To Ali Imran, Toong Way Yun, Lim Lih Wei, Saipul Fakir and Mohd Arif, I am especially grateful for the experience, ups and downs that we have been through together. Not forgetting the senior members of the lab who have guided me, contributing ideas and knowledge: Richard Ritikos, Goh Boon Tong and Gan Wee Chen, all of your contribution to my work and experience will not be forgotten.

I would like to thank my family for all their love, encouragement and support: My wife Afnadia, daughter Batrisya and son Zarif, you are the reason I'm taking this road, to be a much better person, husband and father. For my parents who raised me with a love and supported me in all my pursuits: My mother Badariah Mat Isa and father Yusli Bin Ghali, and to my sisters Roslinda, Yusnita and Noor Akmar, thanks for all the love, support, encouragement all these years.

Mohd Nizam Bin Yusli
University of Malaya
May 2013

Contents

Chapter 1: Introduction

1.1	Research Background on Organic Solar Cells	2
1.2	Research Motivation	3
	1.2.1 <i>Renewable Energy</i>	
	1.2.2 <i>Alternative to Inorganic Solar Cells</i>	
	1.2.3 <i>Advantage of Organic Solar Cells</i>	
1.3	Materials Used in This Study	8
1.4	Research Objective	9
1.5	Outline	10

Chapter 2: Literature Review

2.1	Introduction	12
2.2	Conjugated Polymers	14
2.3	Charge Transport Characteristics of Conjugated Polymers	17
2.4	Basic Principals of Organic Solar Cell	19
	2.4.1 <i>Inorganic and Organic Solar Cells</i>	
2.5	Electrode Interface	24
2.6	Single Layered Organic Solar Cell	27
2.7	Heterojunction Organic Solar Cells	28
2.8	Bulk Heterojunction Organic Solar Cells	30

Chapter 3: Instrument and Experimental Methods

3.1	Introduction	33
3.2	Sample Preparation	33
3.3	Material	35
3.4	Preparation of P3HT, PCBM and P3HT:PCBM blend solutions	35
	3.4.1 <i>Effect of Annealing Temperature</i>	
	3.4.2 <i>Effect of Slow Formation of the Thin Layer</i>	
	3.4.3 <i>Effect of Solvent on The properties of P3HT:PCBM Blend Film</i>	
3.5	Substrate Cleaning	37
3.6	Spin Coating Technique	37
3.7	Aluminum Electrode Deposition	39
3.8	Thickness Measurement	41
3.9	Thin Film and Device Characterization	41
	3.9.1 <i>Ultraviolet – Visible-Near infrared Spectrophotometer</i>	
	3.9.2 <i>X-ray Diffraction Measurement</i>	
	3.9.3 <i>Atomic Force Microscopy</i>	
	3.9.4 <i>Raman Spectroscopy</i>	
	3.9.5 <i>Current-Voltage Characteristic</i>	

Chapter 4: Results and Discussion

4.1	Effect of Annealing Temperatures	52
4.1.1	<i>UV-Vis absorption measurement</i>	
4.1.2	<i>Photoluminescence (PL) Spectra</i>	
4.1.3	<i>X-ray Diffraction Spectra</i>	
4.1.4	<i>Summary</i>	
4.2	Effect of Slow Formation of the Thin Layer	62
4.2.1	<i>UV-Vis absorption measurement</i>	
4.2.2	<i>X-ray Diffraction Spectra</i>	
4.2.3	<i>Raman measurement</i>	
4.2.4	<i>Atomic Force Microscopy</i>	
4.2.5	<i>Current Density-Voltage Characteristic</i>	
4.2.6	<i>Summary</i>	
4.3	Effect of Solvent on the properties of P3HT:PCBM Blend Film and Photovoltaic devices	73
4.3.1	<i>UV-Vis absorption measurement</i>	
4.3.2	<i>X-ray Diffraction Spectra</i>	
4.3.3	<i>Atomic Force Microscopy</i>	
4.3.4	<i>Current Density-Voltage Characteristic</i>	
4.3.5	<i>Summary</i>	

Chapter 5: Conclusion

Conclusion	85
------------	----

List of Figures

- Figure 2.1:** Structure of a bilayer heterojunction organic solar cell. 13
- Figure 2.2:** Structure of a bulk heterojunction organic solar cell. 13
- Figure 2.3:** Chemical structure of Conjugated polymer: (a) polyacetylene and (b) polythiophene 16
- Figure 2.4:** The schematic diagram of HOMO and LUMO bands. The Highest Occupied Molecular Orbital (HOMO) produces from the lower energy π -orbital while the Lowest Unoccupied Molecular Orbital (LUMO) produces from the higher energy π -antibonding (π^*) orbital. 16
- Figure 2.5:** Schematic representation of (a) intrachain charge diffusion and (b) interchain charge diffusion in polyacetylene 17
- Figure 2.6:** Schematic diagram of an organic light emitting diode (a) and an organic solar cell (b). Both are sandwiched between two metal electrodes. In organic solar cells, aluminum, calcium and magnesium are some example used as an electron collector and ITO is usually used as hole collector. As for the LED, electron is introduce at the metal cathode electrode that will recombine with hole introduce from anode electrode, ITO. 19
- Figure 2.7:** Light harvesting in organic solar cells. During radiation, electron is excited to the LUMO creating hole at HOMO. Electron then jump to the metal electrode and hole to the ITO. Φ_{ITO} , Φ_{Al} , E_{ca} , E_{I} , and E_{g} is the ITO workfunction, Al workfunction, electron affinity, ionization potential and energy gap respectively. 21
- Figure 2.8:** (a) The open circuit condition, (b) short-circuit condition in an insulating organic material, (c) short-circuit condition for a hole-conducting polymer. 21
- Figure 2.9:** I-V curve of an organic solar cell under dark (left) and under light illumination (right). 24
- Figure 2.10:** Schematic of a Schottky contact for doped material between the low workfunction electrode and the single layer p-type organic material. Photogenerated exciton diffusion is only limited to the thin depletion region. 27
- Figure 2.11:** Schematic of a heterojunction device shows the exciton dissociated at the donor-acceptor interface. The donor adjacent with the higher workfunction electrode whiles the acceptor with the lower workfunction electrode, to achieve good electron and hole collection, respectively. 29

Figure 2.12:	Schematic of bulk heterojunction device. The donor and acceptor is blend together throughout the whole film. Photogenerated exciton can be dissociated into charges at any place.	30
Figure 3.1:	Photovoltaic Device Architecture	34
Figure 3.2:	The chemical structure of P3HT and PCBM	34
Figure 3.2:	Schematic step by step of the spin coating technique	38
Figure 3.4:	Schematic diagram of the thermal evaporation system.	39
Figure 3.5:	Vacuum chamber schematic diagram.	40
Figure 3.6:	The schematic diagram of the components of a UV-Visible/NIR spectrophotometer.	44
Figure 3.7:	The visible spectrum with respect to infrared and ultraviolet radiation.	45
Figure 3.8:	Block Diagram of Atomic Force Microscope	46
Figure 3.9:	Schematic setup for the current-voltage measurement	49
Figure 4.1.1:	Absorption coefficient spectra of P3HT:PCBM blend film with different annealing temperature	54
Figure 4.1.2:	The plot of $(\alpha h\nu)^2$ vs $h\nu$ of P3HT:PCBM P3HT:PCBM blend film with different annealing temperature	55
Figure 4.1.3:	Photoluminescence spectra of P3HT, PCBM, pristine blend and annealed sample at 125 °C	57
Figure 4.1.4:	X-ray Diffraction spectra of P3HT, pristine blend film and annealed sample at 125 °C.	59
Figure 4.2.1:	UV-vis absorption spectra of P3HT:PCBM blend film.	63
Figure 4.2.2:	X-ray Diffraction of P3HT:PCBM blend film.	64
Figure 4.2.3:	Influence of film formation types on Raman spectra of P3HT:PCBM blend films, (a) Raman shift from 200 to 2000 cm^{-1} (b) enlarged Raman shift from 1350 to 1490 cm^{-1} .	68

Figure 4.2.4:	2D and 3D atomic force microscopy images of (a) As Deposited, (b) Fast Grown and (c) Slow Grown sample.	70
Figure 4.2.5:	J-V plots for P3HT:PCBM solar cells prepared As Deposited, Fast Grown and Slow Grown.	72
Figure 4.3.1:	Absorption coefficient spectra of P3HT:PCBM blend films which were dissolved in pure DCB solvent, pure CH solvent and DCB:CH co-solvent.	75
Figure 4.3.2:	The plot of $(\alpha h\nu)^2$ vs $h\nu$ of P3HT:PCBM blend films which were dissolved in pure DCB solvent, pure CH solvent and DCB:CH cosolvent.	76
Figure 4.3.3:	X-ray Diffraction of P3HT:PCBM blend films prepared in pure DCB, CH and DCB:CH co-solvent.	77
Figure 4.3.4:	2D and 3D atomic force microscopy images of P3HT:PCBM blend films dissolved in (a) pure DCB solvent, (b) CH solvent, and (c) DCB:CH cosolvent	80
Figure 4.3.5:	J-V plots for P3HT:PCBM solar cells prepared in DCB, CH and cosolvent. The inset shows the structure of ITO/PEDOT:PSS/P3HT:PCBM/Al solar cell device.	82

List of Tables

Table 4.1.1:	Variation of absorption with annealing temperature	54
Table 4.1.2:	Variation in the interplanar distance and the crystalline thickness for the P3HT, Pristine and Annealed samples.	59
Table 4.2:	Summary of the interplanar distance and the crystalline thickness for the as deposited, fast grown and slow grown film sample.	66
Table 4.3.1	: Variation of absorption with annealing temperature	75
Table 4.3.2:	Summary of the interplanar distance and the crystalline thickness for the DCB solvent, CH solvent and DCB:CH cosolvent.	78
Table 4.3.3:	The comparison of device characteristic parameters for P3HT:PCBM solar cells with active layers prepared in pure DCB, CH and DCB:CH cosolvent.	83

Chapter One

INTRODUCTION

Introduction

1.1 Research Background on Organic Solar Cells

The research on organic solar cell has started as early as the 19th century with the observation of photoelectrochemical process. However only in the 1950s, the first real investigation on organic solar cell took place. Even so, up to the 1980s, the power conversion efficiency (PCE) organic solar cells based on dyes of polymer were still below 0.1% except for merocyanine dyes that reached 0.7% (Ghosh et al., 1978). In 1986, Tang makes a major breakthrough by combining a donor and an acceptor together in one cell, which dramatically increases the efficiency to 1% (C.W. Tang, 1986). Since then, the research on organic solar cell has developed rapidly. The introduction of new materials and more analytical devices are some of the major incentives which have helped these scientists in their research. A device fabricated by Mitsubishi Chemical has been reported to has set a new efficiency of organic solar cell with PCE of 10% (Green et al., 2012). Although this is not as high as inorganic counterpart, but the lower cost production compared to inorganic material, motivates the research in this area. Highest power conversion efficiency so far at 10.6% for device with tandem structure (You et al., 2013).

1.2 Research Motivation

1.2.1 Renewable Energy

The crisis of conventional energy nowadays has pushed the research to convert solar energy to electrical energy more rapidly. An increase of fuel price for the past few years in the international market has created awareness among the global community for getting more cost-effective renewable energy resources. The research for other sources of energy such as solar cell technology has become crucial as the crisis of conventional energy in the world become more critical. This renewable energy sooner or later will unquestionably replace today main energy source such as petroleum, coal and uranium. Studies have predicted there will be a decline of petroleum production rate for the next 10-20 years (Campbell, 1998; Hatfield, 1997). Global community are aware of these crisis and thus, it will be easier for them to accept the introduction of various renewable energy sources such as wind-power, hydroelectric energy and the direct conversion of solar energy using solar cells.

Carbon dioxides (CO₂) gas created from fossil fuel combustion also brings much harm to the environment. The total amount of plant we have today cannot compensate the huge amount of CO₂ emission. The natural balance of our planet is at risk with the uncontrollable increase of CO₂ gas. Environmental issues from this problem such as greenhouse effect increase the mean surface temperature of our planet roughly 0.3-0.6°C since the late 19th century (*Warm global temperatures continue in 2011*, 2011). Global warming as we call it is not a false threat, it is actually happening. And this brings to the increase of global sea level and other climate change which spell for disaster.

Luckily there is other way to obtain energy source that is renewable, which never run out and have no harmful effect to the environment. These kinds of energy source harvest the natural potential of the planet to produce electrical energy. Solar energy, wind, tidal wave, river dam and heat from the earth crust are some of the example of renewable energy. Even though that this energy source can supply for a longer period of time, there is some major drawback. These energy sources need potential spaces or places for it to be effective, and the amount power they can supply depend on the geographical and weather condition. And also, the power plants are very expensive to be build and maintained. The power that these power plants can supply in their lifetime should compensate the fabrication, installation, and maintenance. Even though that these power plants can resolve the problem mention above, the cost is not low enough.

Because the cost to build and sustain this kind of renewable energy source is too high, a new kind of renewable energy need to be develop. Research need to be done to find energy source that is not too dependable to the geographical surface and can be place anywhere. The research also needs to be concentrated to a more flexible system as the world is moving toward high-technology community. Environmental friendly system is also need to be considered.

1.2.2 *Alternative to Inorganic Solar Cells*

Nowadays, inorganic material such as silicon is leading the way in solar cell technology. Mono and multi-crystalline silicon have been widely used and can be found in every day device such as pocket calculator, solar panels on roofs, street light and even on electric cars. Today, silicon based solar cells is the most dominating type of solar cells used and account for 99% of all the solar cells (Hatfield, 1997). With efficiency of the devices peaks up to more than 25% (Green, et al., 2012) and theoretical value predicted to be more than 30% (Shockley et al., 1961), inorganic solar cells has become the most favorable way to harvest energy source in the future. But the manufacturing cost and very difficult to fabricate has become its drawback. We now desire a low production cost rather than a high efficiencies device. There has been an effort to cut the production cost of inorganic solar cells using a minimal amount of silicon by using thinner film on glass substrates, however the fabrication process still require condition at high temperature and high vacuum with cumbersome lithography steps (Skompska, 2010). Even though inorganic solar cell has been leading solar cell technology, the production cost and the complexity of the fabrication process had made researcher to endeavor to replace it with a cheaper, flexible and simpler device.

1.2.3 Advantage of Organic Solar Cells

The polymer based solar cell offers the possibility of low-cost fabrication on a large scale of solar cell harvesting solar energy. Apart from that, these polymer devices have the flexible capability such as light weight and it is mechanically bendable. These factors open up more possibility of other solar cell application in our daily use. Organic material has been widely investigated throughout the decade and considered to be the solution to replace inorganic material to become a high efficiencies solar cell. The research in this field has increased in the past few decades. It has a simpler fabrication process and at lower temperature (28-200°C) compared to the inorganic counterpart. With the introduction of bulk heterojunction concept, the PCE of organic solar cell has increase nearing to 6.5% (Yamanari et al., 2006). With a low production cost, this device will hopefully enter the commercial market in the near future.

Conjugated polymers are a very attractive material which combines the optoelectronic properties of conventional semiconductor with excellent mechanical flexibility and processing properties of polymeric like plastic materials. Typically, conjugated polymer are recognized as conducting polymers, which are distinguished by alternating single and double bonds between carbon atoms on the polymer backbone (Wallace et al., 2000). These types of polymer are organic semiconductors that give a good impact to the development in optoelectronic devices, such as providing an alternative to inorganic photovoltaic devices, since they are strong absorbers and can be deposited on flexible substrates at low cost (Coakley et al., 2004).

Another fine property of these polymeric solar cells which offer the advantage compared to inorganic cells is the mechanical flexibility they possess. The plastic like behavior of these semiconducting polymers allow them to be deposited onto flexible and cheaper substrates using simple processing methods like spin coating technique from the materials solution. Thus, organic solar cells can be used on curvature surface such as tent, traveling bags, and other flexible surface. However, the PCE value is still low compared with inorganic solar cell, especially silicon based solar cell. The device having a shorter life time also limits the usage of the organic solar device and prevents it to be widely commercialized. Nevertheless, there are many research works have been carried out to improve the life-cycle.

1.3 Materials Used in This Study

Poly(3-hexylthiophene) (P3HT) and [6,6]-phenyl-C61-butyric acid methyl ester (PCBM) has become a favorable materials as it has shown good potential and has been widely investigated as an active layer in organic solar cell based on bulk heterojunction concept (Al-Ibrahim et al., 2005; Jin et al., 2007; Vanlaeke, Swinnen, et al., 2006; Yamanari, et al., 2006; Yang et al., 2005). P3HT has been the mostly used p-type material in along with a fullerene derivative, PCBM as an electron acceptor. These blends have shown a promising result and has the highest performance to date compared to other materials. P3HT possesses some unique properties over other polymers including its high self-organization capability, high holes mobility, and extended absorption in the red region. Since hole is typically the high-mobility carrier in P3HT, the enhanced electron mobility is achieved by addition of electron acceptor, PCBM. Many approaches have been taken to improve the efficiencies of the solar cell. By thermal annealing process, the morphology and optical properties of the device can be improved (Vanlaeke, Swinnen, et al., 2006; Yamanari, et al., 2006).

1.4 Research Objective

This study aims to prepare the thin films based on poly(3-hexylthiophene) (P3HT)/[6,6]-phenyl-C61-butyric acid methyl ester (PCBM) mixture. The prepared thin films are then characterized for their optical, structural as well as surface morphology. Subsequently, the BHJ solar cells are fabricated utilizing the mixture of P3HT/PCBM film as active layer. The photovoltaic properties are then characterized in the dark as well as under light illumination. Three physical parameters will be used to vary the properties; first is the thermal annealing temperature; secondly, the solvent treatment and finally the solvent used in the material preparation.

Thus the objectives of this research can be categorized as:

- i. To investigate the influence of annealing temperature on the optical, structural and morphological properties of P3HT:PCBM thin films as well as on the electrical behaviors of the fabricated devices.
- ii. To study the influence of solvent treatment on the optical, structural and morphological properties of P3HT:PCBM thin films as well as on electrical behaviors of the fabricated devices.
- iii. To examine the effect of solvent in material preparation, on the optical, structural and morphological properties of P3HT:PCBM thin films as well as on electrical behaviors of the fabricated devices.

1.5 Outline

Chapter 2 is aimed to introduce reader to the theoretical understanding of organic solar cells. It consist the overview of the research and review of other work that has been done in this field that will be used as a guideline. The related theory of this research work which is divided to few sub topics. The sub topics included the literature review, conjugated polymer, and charge transport characteristic and so forth. The history of organic and polymeric solar cell is also highlighted.

Chapter 3 explains the experimental methods of this project work. The chapter includes the preparation of the sample; spin coating technique and thermal evaporation process. The characterization using Ultraviolet-Visible/Near Infrared (UV-Vis/NIR) spectroscopy, Atomic Force Microscopy (AFM), Raman Spectroscopy, X-ray diffraction measurement (XRD), and current density-voltage (J-V) is explained.

Chapter 4 explains the results and discussions on optical and morphological characterization of the blend film thin films. The charges in properties of the thin films are discussed. Optical characterization is defined using optical result of UV-Vis/NIR. The changes in morphological properties for blend films are explained using result of AFM imaging. The crystallinity of the thin blend films is detected using XRD measurement.

Finally, chapter 5 concludes the overall research and also suggests some future work that can be carried out related to this research.

Chapter Two

LITERATURE REVIEW

Literature Review

2.1 Introduction

In the early days, organic solar cell was based on single active layer sandwiched between two electrodes with different work functions. The power conversion energy of a single layer solar cell is limited by the surface of the electrode/organic contact. With the discoveries of the heterojunction solar cell, where double layered device of donor/acceptor is used, the architecture of these devices has been enhanced. The main benefit of this structure is the separation of charge transport layers that ensure connectivity with the electrode.

The concept of heterojunction device is based on the usage of two materials with different electron affinities and ionization potentials. In bilayer heterojunction device, two organic films are stacked together between two electrodes as shown in Figure 2.1. On the other hand, the donor and acceptor is blend together in bulk/dispersed heterojunction device as shown in Figure 2.2. Tang discovered the first organic solar cell consisting of copper phthalocyanine and perylene derivative has a PCE of 1% (C.W. Tang, 1986). Consequently in 1991, Hiramoto used a dye/dye-dispersed with the same class of donor and acceptor as Tang did with an additional third layer in the organic solar cell between the two layered heterojunction (Hiramoto et al., 1991; Hiramoto et al., 1992). It was found that the photocurrent was double as compared to the two layered device. The first dispersed heterojunction was made by Yu in 1994 (Yu et al., 1994). A solution of poly(2-methoxy,5-(2'ethyl-hexyloxy)-1,4-phenylene vinylene) (MEH-PPV) and buckminsterfullerene (C_{60}) was spin coated onto Indium-tin-oxide (ITO) glass with 10:1 weight-ratio. Calcium (Ca) was then evaporated

to the organic layer. The cell showed a photosensitivity of 5.5 mA/W, an order of magnitude larger than the photosensitivity of the pure polymer.

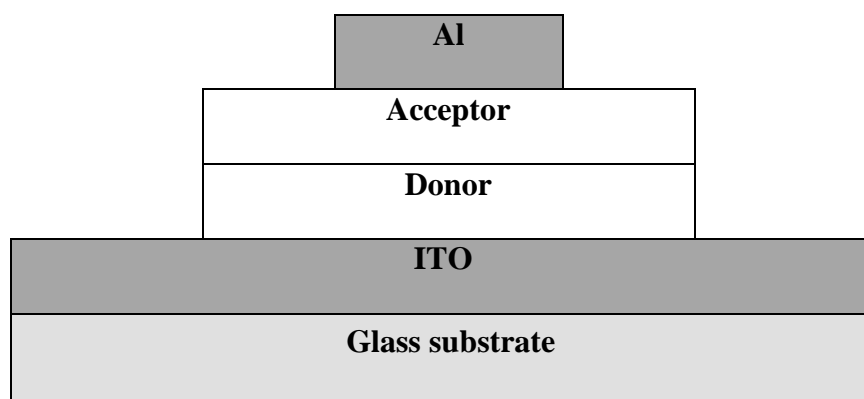


Figure 2.1: Structure of a bilayer heterojunction organic solar cell.

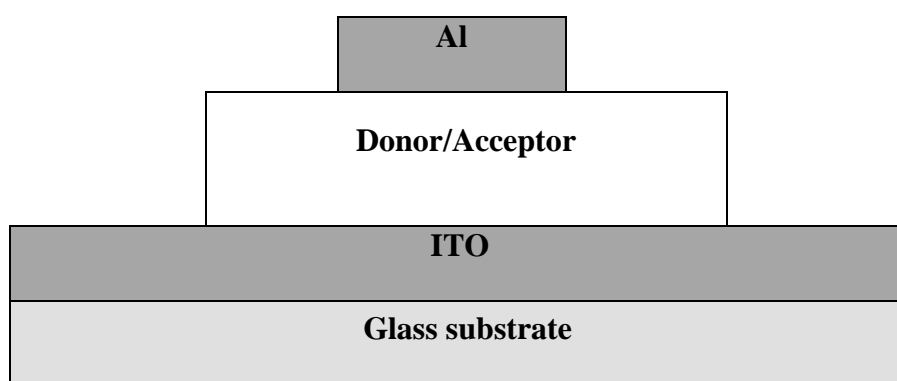


Figure 2.2: Structure of a bulk heterojunction organic solar cell.

2.2 Conjugated Polymers

A conjugated polymer is a polymer consists of a “sigma” (σ) bond with a “pi” (π) bond network extending along the polymer chain (Kalinowski, 1999). They can be easily recognized because they possess a structure of alternating single and double bonds (Skotheim, 1998) as shown in Figure 2.3. Every single bond contains a localized σ -bond which is a strong chemical bond and double bond contains a less strongly localized π -bond together with σ -bond. For an organic molecules, it consist two fundamental types of carbon bond hybridization, which are sp^3 and sp^2 . For an example, we consider ethylene, each carbon atom in a molecule forms three σ -bonds having C-H and C-C bonds (Nunzi, 2002). Hence, each carbon atom has an unbounded valence electron that will pair up to balance the valence electron in order to achieve full outer shell. With that, a second covalent bond between the two carbon atoms is built. Accordingly, the atoms are required to alter the orbital structure of their p orbitals to accommodate the existence second C-C bond. The presence of the final two electrons in p_z orbitals causes the electrons in the bond to have a less tightly bound to the carbon nuclei. This is termed as π bond which can be considered to be a more delocalized entity (Petty et al., 1995). The characteristic of π bonds are the source of the semiconducting properties of these polymers. In an ideal semiconductor, the electronic structure consists of a conduction band and a valence band separated by an energy gap, the size of which depends upon the materials shown in Figure 2.4. Conjugated polymers are organic semiconductors which have the electronic properties that appear to be similar to those of inorganic semiconductors.

The quantum mechanical overlap of p_z orbitals actually produce two orbitals, a full π -bonding orbital and an empty π -antibonding (π^*) orbital which are analogous to the valence band and conduction band for typical semiconductor. Figure 2.4 shows the lower energy π -orbital produces the Highest Occupied Molecular Orbital (HOMO), while the higher energy π -antibonding (π^*) orbital forms the Lowest Unoccupied Molecular Orbital (LUMO) (Hiramoto, et al., 1992). Electrons in these π bonds are less tightly bonded to the carbon nuclei, and thus they require less energy to excite across energy gap between the valence and conduction band (Petty, et al., 1995). The difference in energy between the two bands produces the band gap that determines the optical properties of the material. Most semiconducting polymers can be used in optoelectronic devices that work in the optical light range since they have a band gap lies in the range 1.5-3.0 eV (Wallace, et al., 2000).

Electronic properties of polymers can be described in terms of semiconductor physics (Kittel, 1972). The basic understanding of an isolated polymer chain can be a good explanation for the particular framework of one dimensional periodic media (Cojan et al., 1977). As π -orbitals overlap is weaker than σ -orbitals overlap, the energy band gap between bonding and antibonding molecular orbitals is larger for the π - π^* difference than for the σ - σ^* molecular orbitals. The π - π^* molecular orbitals are more concerned in this respect. Those are the HOMO and LUMO respectively, in terms of molecular physics. σ -bonds then only contribute to the stability of the molecular structure (Su et al., 1979). Due to the delocalization of chemical bonding, conjugated polymers possess electrical conductivity (Roth et al., 2004).

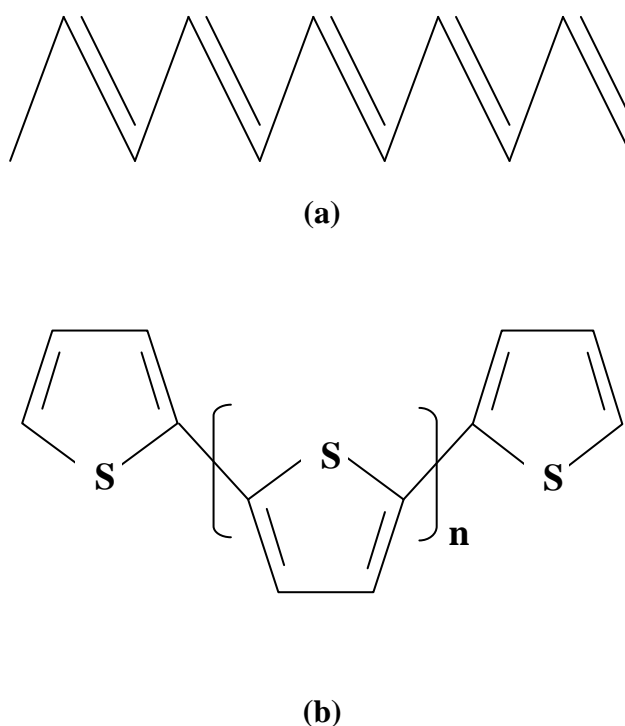


Figure 2.3: Chemical structure of Conjugated polymer: (a) polyacetylene and (b) polythiophene

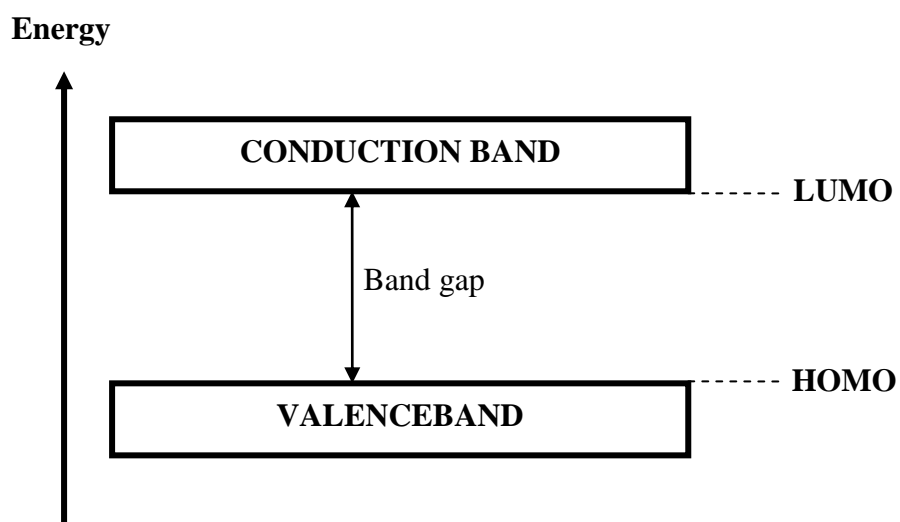


Figure 2.4: The schematic diagram of HOMO and LUMO bands. The Highest Occupied Molecular Orbital (HOMO) produces from the lower energy π -orbital while the Lowest Unoccupied Molecular Orbital (LUMO) produces from the higher energy π -antibonding (π^*) orbital.

2.3 Charge Transport Characteristics of Conjugated Polymers

The charge transport characteristics of conjugated polymers are for the most part governed by the polymer backbone itself; however the existence of intermolecular interactions can drastically influence the macroscopic materials properties too. Charge transport process of conjugated polymers relatively depends on their charge carrier mobility. Charge carriers with higher mobility can be easily transported than those with lower mobility. The charge carrier mobility of conjugated polymers is a function of intrachain charge diffusion and interchain interactions (Brabec et al., 2001; Horowitz, 1998; Mark, 1996; Nalwa, 1996; Skotheim, 1998), for example, hopping as shown in Figure 2.5. Intrachain charge diffusion depends on the chemical structure and the molecular weight of polymer, conformation of the polymer backbone, the number and nature of defect sites. While, the interchain interactions governed by the degree of contact, order and orientation (Cao et al., 1989).

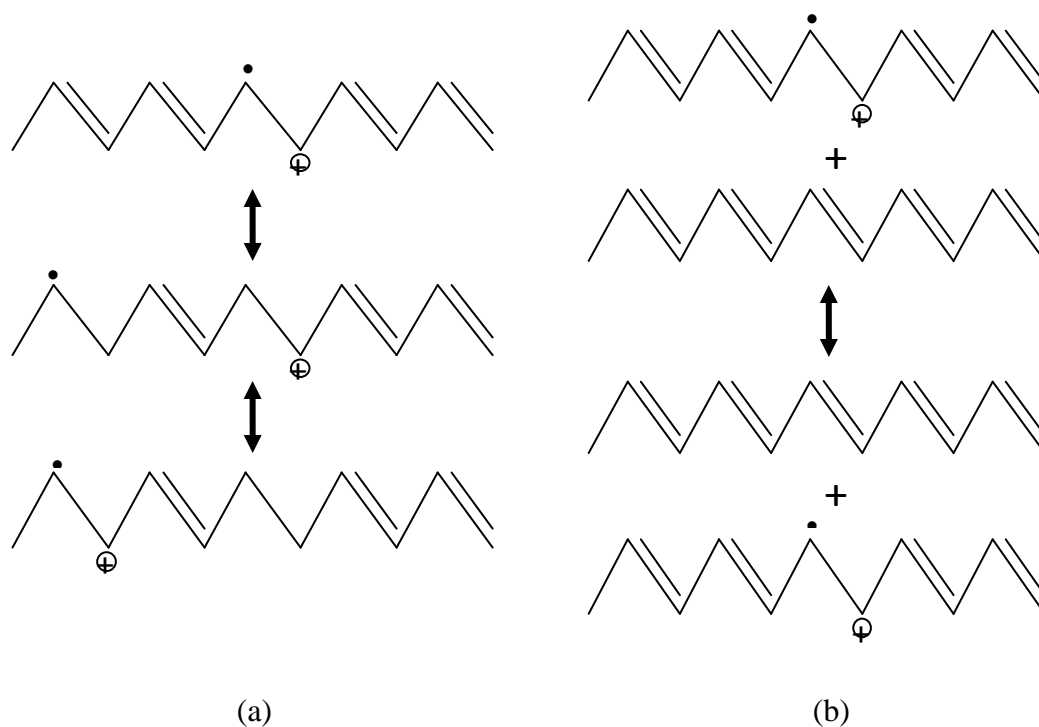


Figure 2.5: Schematic representation of (a) intrachain charge diffusion and (b) interchain charge diffusion in polyacetylene.

Recently it was reported that the increase of the charge carrier mobility with increasing molecular weight coincided with the amount of overlap between the ordered regions of the film. It was demonstrated for low-molecular-weight poly (3-alkylthiophene), P3ATs that the induced orientational order (thus the overlap) between aggregates is low when processing them under low temperature. However, the charge carrier mobility was observed to increase if these films were annealed, this was due to the better ordering and overlap between aggregates (Chang et al., 2004). More recent studies have shown that the charge carrier mobility can be greatly enhanced in ordered, organized structures due to improved interchain hopping. Regioregular P3HT was chosen in many research works related to its optoelectronic properties since it has the highest charge carrier mobility among the conjugated polymers and its hole mobility is reported as high as $0.1 \text{ cm}^2/\text{V}\cdot\text{s}$ (Sirringhaus et al., 1998). The excellent mobility of P3HT is due to its tendency to self-organize into highly ordered lamellae that lead to strong interchain interactions and favor efficient charge transport between the chains (Jiang et al., 2002; Sirringhaus et al., 1999).

Another technique to enhance the charge transport is at the active layer of the electrode, by increasing the inter-penetrating network as evident by the coarser surface mean roughness. Rougher surface yields a greater phase separation and a larger interfacial area for excitons dissociation (L. M. Chen et al., 2009; Li et al., 2007; Wang et al., 2012; Yao et al., 2008). Furthermore, this phase separation also develops a continuous pathway for charge carrier to move to its respective electrodes (Kwong et al., 2004).

2.4 Basic Principals of Organic Solar Cell

The structure of most organic solar cell is planar-layered where the organic material is sandwich between two electrodes with different workfunction. One of the electrodes is semi-transparent for the light to get to the organic layer. Indium-tin-oxide (ITO) is usually used, but a thin metal layer can also be used. The other electrode is metal, usually aluminum, calcium, magnesium, aurum et cetera. Fundamentally, the basic principal of an organic solar cell (sometimes call organic photovoltaic cell) is that it works reversely with the principal of light emitting diodes (LEDs) as shown in Figure 2.6. The research and development of organic solar cells and LEDs are somewhat related.

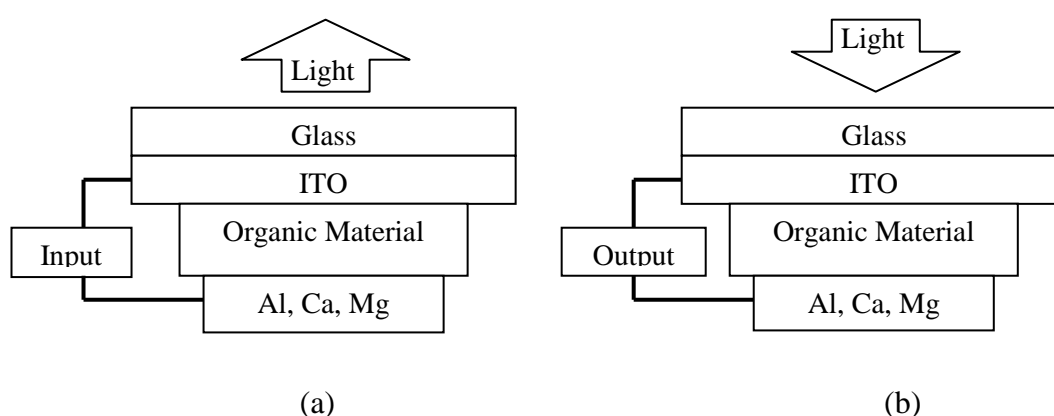


Figure 2.6: Schematic diagram of an organic light emitting diode (a) and an organic solar cell (b). Both are sandwiched between two metal electrodes. In organic solar cells, aluminum, calcium and magnesium are some example used as an electron collector and ITO is usually used as hole collector. As for the LED, electron is introduced at the metal cathode electrode that will recombine with hole introduce from anode electrode, ITO.

In LEDs, electron is introduced at the low-workfunction electrode (cathode) with the balanced introduction of hole at the high-workfunction electrode (anode) and when the electron and hole met, it produce a light from the recombination of the electron and hole in the cell. Similar thing happens in organic solar cell but only in a reverse process where the electron is flowing from anode to cathode when a there is a light introduced to the cell. Figure 2.7 show the energy level upon light radiation for organic solar cells. The light that been absorb by the solar cell excite the electron from the highest occupied molecular orbital (HOMO) to the lowest unoccupied molecular orbital (LUMO) forming an exciton. Exciton dissociation must occur after this process for the solar cell to work. The electron charge must reach one electrode and hole must reach the other. For this to happen, the charge carriers need a driving force which come from the uneven workfunction. The uneven workfunction of the two electrode work as an electrical field and help to achieve charge separation in the cell. In other word, the processes of converting light into electrical current consist of:

- 1) Absorption of photon, leading to the formation excited state, electron-hole pair (exciton).
- 2) Exciton diffusion to a region, where the charge separation occur.
- 3) Charge transport, hole to the anode electrode and electron to cathode electrode.

This process will continue as light bombarded the cell resulting in a current in the circuit.

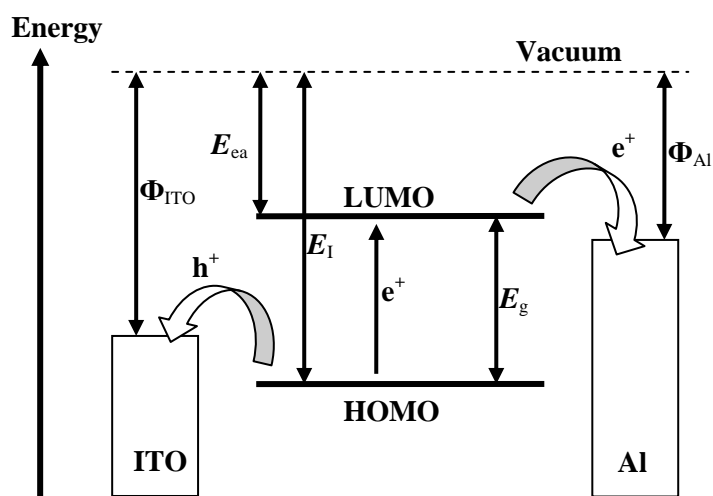


Figure 2.7: Light harvesting in organic solar cells. During radiation, electron is excited to the LUMO creating hole at HOMO. Electron then jumps to the metal electrode and hole to the ITO. Φ_{ITO} , Φ_{Al} , E_{ea} , E_{i} , and E_{g} is the ITO workfunction, Al workfunction, electron affinity, ionization potential and energy gap respectively.

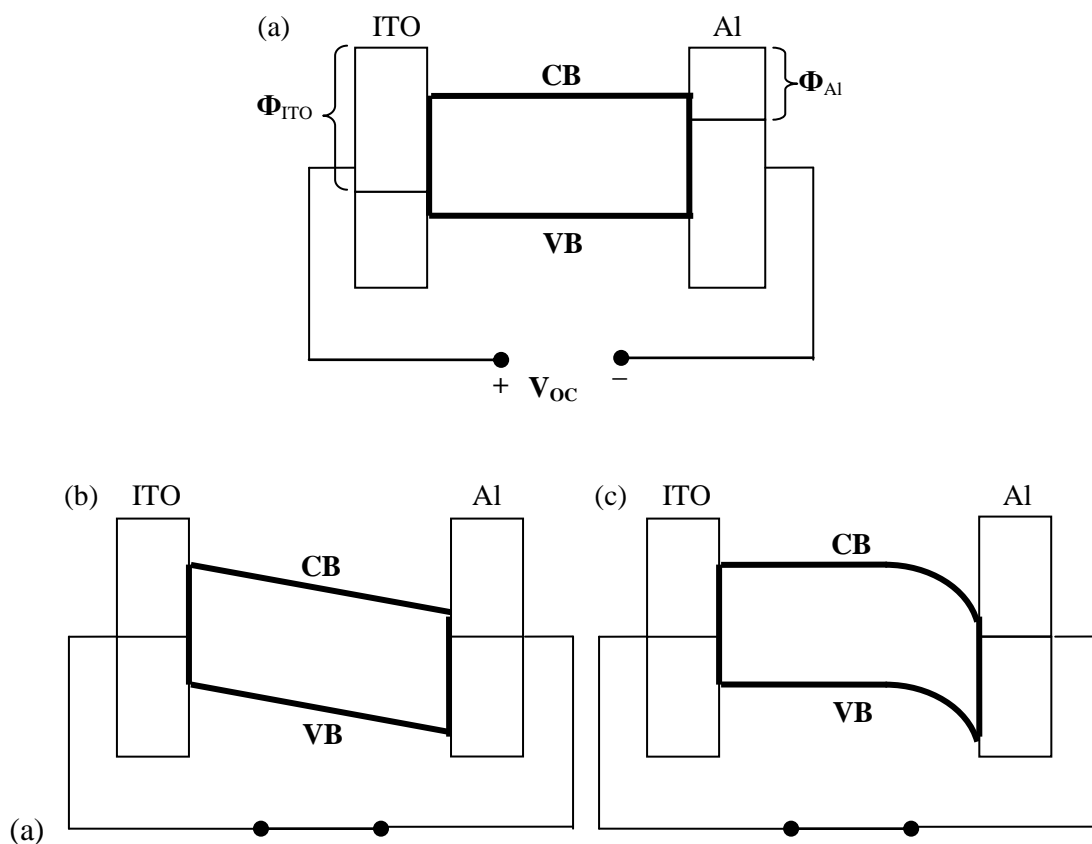


Figure 2.8: (a) The open circuit condition, (b) short-circuit condition in an insulating organic material, (c) short-circuit condition for a hole-conducting polymer.

Depending on several situations, HOMO and LUMO of molecules will form conduction (CB) and valence band (VB) respectively. In Figure 2.8, several situation of organic materials sandwiched between two electrodes with different workfunction is depicted. The CB and VB will change depending on the conductance and whether the electrode is connected. The open circuit condition is shown on Figure 2.8(a), in the dark condition. This condition is also known as the ‘flat band condition’, where the voltage apply is label as open-circuit voltage (V_{OC}). The different in the build in field from the electrodes workfunction is level out by the voltage applied. The current is zero, as there is no driving force for the charge carrier. Figure 2.8(b) is presented to represent the short-circuit condition in an insulating organic material giving in a field shape that changes linearly though the material. There is no net current flowing, and the metal’s workfunction causes the build-in electric field to be evenly distributed throughout the device. When the device is illuminated, the separated charge carrier will drift to the respective electrode (electron to the low workfunction electrode and hole to the high workfunction electrode). In Figure 2.8(c), the situation is shown for a hole-conducting polymer is used in a short-circuit condition, when the device is illuminated. The generated holes are permitted to dispense liberally due to the p-conduction properties, and they will even out the band approaching the high workfunction electrode forming a Schottky junction. The curvature form which the CB and VB exhibit is call depletion region.

2.4.1 Inorganic and Organic Solar Cells

The fundamental difference between inorganic semiconductor and inorganic dye semiconductor is that in a crystalline inorganic semiconductor with the 3D crystal lattice the individual LUMOs and HOMOs create a CB and VB throughout the material whereas most of the organic dye semiconductor molecular force is too weak to create a 3D crystal lattices. Therefore, the molecular LUMOs and HOMOs do not interact strongly to create a CB and VB. Rather than transport within the band, the charge transport proceeds by hopping between localized states. This means that the charge carrier of the organic and polymeric semiconductors is in general lower compared to inorganic semiconductors. Low dielectric constant in organic semiconductor also makes it difficult for charge separation to occur. In most inorganic semiconductors, photon absorption produces a free electron and a hole, whereas for organic semiconductor, the excited electron is bound to the hole to form exciton. Conjugated polymers lie somewhat between inorganic semiconductor and organic dye semiconductor.

Exciton dissociation in organic solar cells and diodes based on organic device occurs at the electrode interface. If the organic layer is too thick, the exciton that is created in the middle of the organic layer cannot reach the electrode interface and hence recombine. By increasing the layer thickness, it will reduce the number of absorbed photons.

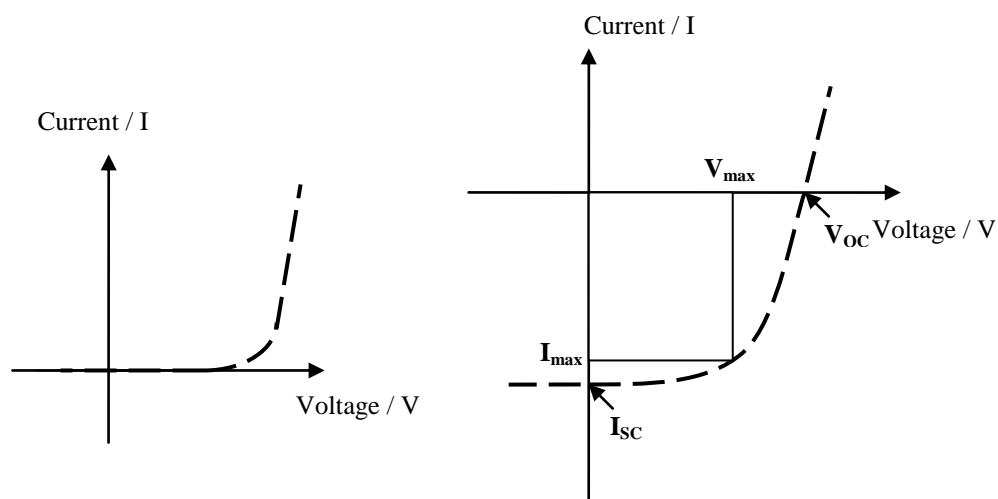


Figure 2.9: I-V curve of an organic solar cell under dark (left) and under light illumination (right).

2.5 Electrode Interface

The injection and photovoltage critically depend on the interface of the electrodes. When a pristine conjugate polymer is brought into contact with an electropositive metal electrode such as aluminum, calcium, magnesium et cetera, the interface is never sharp. Generally, the bigger interface resistant, the injection of the electron or hole to the collecting electrodes becomes harder. For an example, poly(*p*-phenylenevinylene) on aluminum XPS studies reveal that a 30Å thick insulating layer is form between the electrode and organic layer (Spanggaard et al., 2004). This insulating layer is formed when the aluminum atom diffuse with the polymer matrix vinyl group and disturbed the conjugation. This layer causes the increase of the barrier effect and the resistant for electron injection at the interface. As the insulating layer becomes thicker, hence the making extraction of electron impossible creates a useless device. Some methods have been proposed to overcome this problem. A thin interfacial layer such as LiF is placed between aluminum electrode and organic layer is already been used to reduce this electron –injection barrier in LED type devices. Hung *et al.* has demonstrated that a 5–10Å thin LiF or MgO layer improved efficiency of the aluminum-electrode by

lowering the electron-injection barrier (Hung et al., 1997). Greczynski and co-worker has proven that LiF does not dissociate and react chemically, but rather serves as a protecting layer between the electrode and the organic material of polyfluorene (Greczynski, 1996). Very recently Brabec et al. have shown that the advantages of using a protective layer on the negative metal electrode carry well over in organic solar cell devices (Brabec et al., 2002). Without a doubt, LiF has the ability to lower the cathode workfunction and improve the contact efficiency. Furthermore, Al₂O₃ has been shown to have favorable properties as a protective layer reducing drive voltage and increasing device performance in LED type device (H. Tang et al., 1997).

On the other side, the ITO is the material usually use as the high-workfunction electrode in organic solar cell and OLED devices. But the interface between this ITO and organic layer is still not well understood. There is a vast category of ITO morphology and workfunction varying from different manufacture and different batch (Mailis et al., 1996; Pissadakis, 1999; Xirochaki, 1998; Xirouchaki et al., 1996). Rapid polymer degradation is also an issue when there is an uneven surface of ITO on glass. The ITO workfunction could be increased by plasma treatment or by molecular monolayer modification (Moss, 2002; Sugiyama, 2003; Wu et al., 1997). Atomic Force Microscopy (AFM) and Ultraviolet Photoelectron Spectroscopy (UPS) studies have shown that acid etching and ozone cleaning can be used to control the surface (J. S. Kim et al., 1998). Similar to the cathode interface, atoms from the anode can react with the organic material. Therefore in one study it was found that oxygen could diffuse into MEH-PPV forming aromatic aldehydes (Scott et al., 1996). Moreover, indium was found to diffuse into the organic layer where it acts as trapping site for charge carriers (Schlatmann et al., 1996). The introduction of (poly[3,4-(ethylenedioxy)-thiophene]:poly(styrene sulfonate), PEDOT:PSS, is one strategy to reduce the diffusion

of indium and oxygen when it is placed at the interfacial hole-transporting layer. This material has a higher workfunction than ITO will improve the performance of the organic solar cells (Brabec, et al., 2001; T. M. Brown et al., 1999; Gebeyehu et al., 2003; Granstrom et al., 1998; Peumans et al., 2001; Roman et al., 1998). Depending on the state of doping and morphology control from solvent treatment and annealing, its conductivity can reach a high value, assumingly like metal (Jönsson et al., 2003; J. Y. Kim et al., 2002). In addition, the rough surface of ITO can be significantly reduced by inserting this PEDOT:PSS layer.

2.6 Single Layered Organic Solar Cell

At the early stage organic solar cells was based on single organic layer sandwiched between two metal electrodes with different workfunction. The MIM-model can be used to explain this operation for the insulator or the Schottky barrier for doped material between the low workfunction electrode and the p-type organic material (Sze, 2007). In the case of Schottky junction, which close to the contact within the depletion region, a band bending occurs from the Schottky contacts as shown in Figure 2.10.

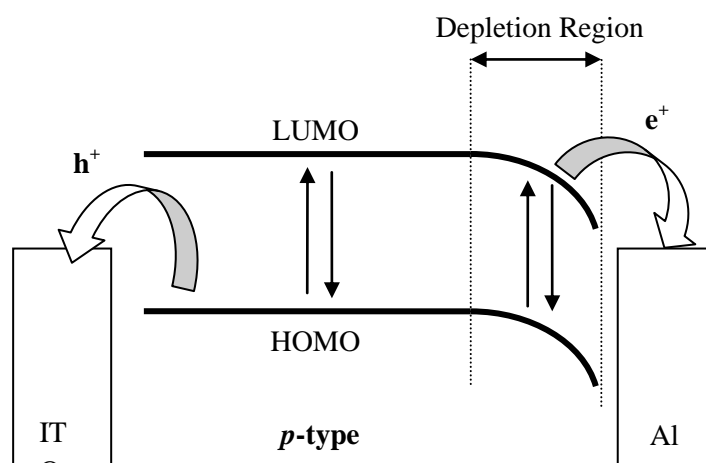


Figure 2.10: Schematic of a Schottky contact for doped material between the low workfunction electrode and the single layer p-type organic material. Photogenerated exciton diffusion is only limited to the thin depletion region.

The exciton can be dissociated resultant to an electric field, where illumination from two different semitransparent metal contacts can lead to symbatic (proportional to the absorption coefficient) and antibatic manners of the spectral photocurrent (C. W. Tang et al., 1975; Wöhrle et al., 1991). Most of organic material diffusion length is below 20 nm, so only those excitons generated in that small region will contribute to the photocurrent. These materials show a low fill-factor and a field-dependant charge carrier collection due to the high series of resistance.

2.7 Heterojunction Organic Solar Cells

In a heterojunction device, a donor and acceptor is piled together with a planar interface. The idea behind it is to use two materials with different electron affinities and ionization potentials. A large potential drop between the donor and acceptor triggered the charge separation (Pettersson et al., 1999; Peumans et al., 2003; Rostalski, 2000). The electron will be extracted by the material with the larger electron affinity and hole will flow to the lower ionization potential. Due to the energy alignment, there is no band bending occurs, and the different in ionization potential and electron affinity of the adjacent material do not require it to be doped like the classical p/n-junction semiconductor. The bilayer is sandwiched between two electrodes corresponding to the donor HOMO and acceptor LUMO, for proficient extraction of the charge carriers. Referring to Figure 2.11, the donor electron is excited from HOMO to LUMO leaving a hole behind. The electron and hole can recombine and creating a luminescence but if there is an acceptor nearby, the electron may jump to the acceptor LUMO, which is more preferable, compared to the donor LUMO, separating it from the hole. Noted that this process needs the excitation energy that obtain from illumination for the electron to reach the LUMO acceptor (photoinduced charge transfer).

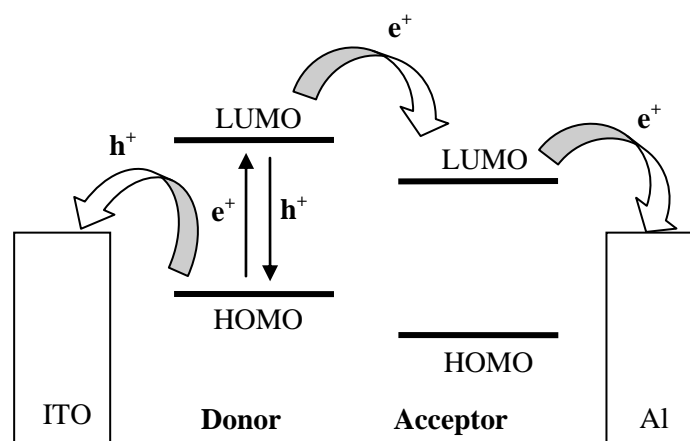


Figure 2.11: Schematic of a heterojunction device shows the exciton dissociated at the donor-acceptor interface. The donor adjacent with the higher workfunction electrode whiles the acceptor with the lower workfunction electrode, to achieve good electron and hole collection, respectively.

Monomolecular charge transfer is the clear advantage of heterojunction compare to single layer device. The recombination is significantly decreased and depend more on trap densities due to the separation of electron and hole. The electron travel inside the n-type acceptor, and hole travel inside the p-type donor material after the excitons are dissociated at the materials interface. The photocurrent is linearly dependent to the illumination intensity (Halls et al., 1997; Halls et al., 1996; Rostalski, 2000; Sariciftci et al., 1993), and a larger fill-factor can be achieved by using a thinner organic layer (C.W. Tang, 1986). Heterojunction device can be deposited either by using thermal evaporation process consecutively one material after another (Hiramoto et al., 1990; Peumans, et al., 2003; Rostalski, 2000; C.W. Tang, 1986), or using solution casting of one soluble material layer and evaporation process for the second layer (Breeze et al., 2002; Halls, et al., 1997; Halls, et al., 1996; Roman, et al., 1998; Sariciftci, et al., 1993).

2.8 Bulk Heterojunction Organic Solar Cells

For a heterojunction device, the exciton dissociation mainly effective at the donor and acceptor interface. Hence, the formation of exciton should be within this diffusion length of the interface. Naturally, the diffusion lengths are in the range of 10 nm, which limit the effective the photoinduce charge transfer process. Planar heterojunction cells must be thin to enable successful diffusion to contacts, but the thinner the cell, the less light it can absorb. The film thickness for organic solar cell is usually around 100 nm in order for the device to absorb enough light. On other word, a thicker cell will allows a large quantity of light to be absorbed, but only a tiny proportion of exciton will reach the interface and dissociate. To resolve this problem, the donor and acceptor can be combined together to form a blending material layer so called bulk (or dispersed) heterojunction cell.

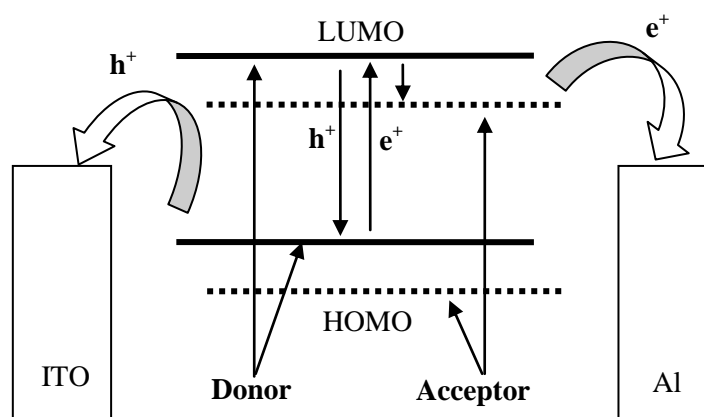


Figure 2.12: Schematic of bulk heterojunction device. The donor and acceptor is blend together throughout the whole film. Photogenerated exciton can be dissociated into charges at any place.

The idea behind mixing the donor and acceptor in bulk heterojunction cell is that the donor-acceptor interface is within a distance less than the exciton diffusion length of each absorbing site where the probability of separation to occur for each of the exciton anywhere in the cell is high. Figure 2.12 shows the schematic of a bulk heterojunction device, where like the bilayer heterojunction device, there is no energy level alignment and interface effect takes place. The concept of donor-acceptor in bulk heterojunction is comparable with bilayer heterojunction device plus a large increase of interfacial area between the donor and acceptor where the charge separation occurs. The interfacial area is dispersed throughout the cell giving to an extremely decrease in recombination loss due to small diffusion length where most of the exciton will be dissociated during their lifetime. This will lead to an increase of photocurrent linearly (Gebeyehu et al., 2004; Schilinsky et al., 2002; Yohannes et al., 2004) or sub-linearly (Dyakonov, 2002; Katz et al., 2001; Yu et al., 1995) with the light intensity. The bulk heterojunction devices are also consider much more sensitive in the nanoscale morphology. The donor and acceptor phase form a bi-continuous and interpenetrating network where a percolated pathways for the hole and electron transporting phase to the electrodes is provided.

The light absorption of an organic material is limited to cover either UV or visible region. Introducing more than one material has made the absorption range covers a broader region of spectrum. It is a good improvement to implement film with this absorption property in photovoltaic device since a broader range of light can be absorbed. Another example of materials which have complementing absorption properties are P3HT:PCBM (Hauch et al., 2008) and DH6T-PCBM-P3HT (Muhammad et al., 2011).

Chapter Three

INSTRUMENTS AND EXPERIMENTAL METHODS

Instruments and Experimental Methods

3.1 Introduction

In this chapter, the experimental methods of fabricating organic solar cells, including the solution preparation and the deposition technique to form a uniform organic thin film, are discussed. The operational principles of the instruments used in this study are discussed. The optical and morphological of the prepared films as well are characterized using UV-visible/NIR Spectrophotometer, Raman Spectroscopy, X-ray diffraction and Atomic Force Microscopy. The set-up of a Source-Measuring-Unit controlled with a personal computer is presented in this chapter, for the measurement of the electrical behaviors of the fabricated devices in the dark. For the electrical characteristics under light illumination, usage of a Solar Simulator is described.

3.2 Sample Preparation

The organic solar cells were arranged in the standard formation where the blend active layer is sandwiched between two electrodes, indium-tin-oxide (ITO, $30 \Omega \text{ cm}^2$) and aluminum (Al). Top electrode of aluminum was deposited later on top of the active layer through a shadow mask using thermal evaporation in ultra-high vacuum (10^{-6} mbar). The photovoltaic device consists of ITO/P3HT:PCBM/Al is shown in Figure 3.1. To fabricate the polymer thin layer, it needs to go through a set of procedures. The sample solution has to be prepared and the substrate needs to be cleaned prior to the film deposition.

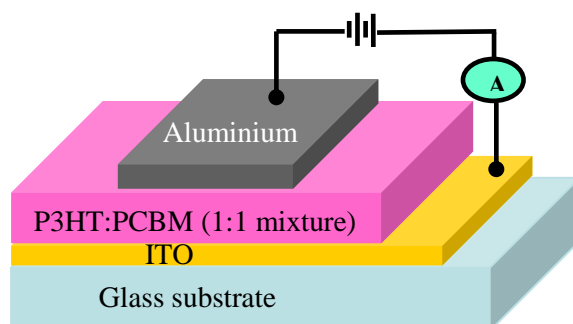


Figure 3.1: Photovoltaic Device Architecture

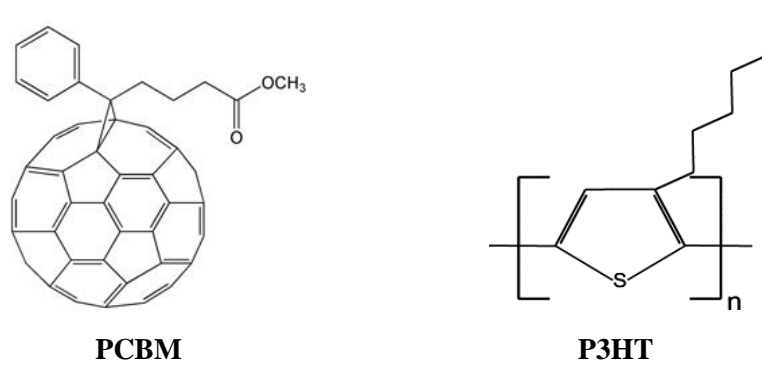


Figure 3.2: The chemical structure of P3HT and PCBM

3.3 Materials

The photoactive layer consist a mixture of regioregular poly(3-hexylthiophene) (P3HT), purchased from Sigma-Aldrich and [6,6]-phenyl-C61-butyric acid methyl ester (PCBM), purchased from American Dye Source, Inc. The chemical structures of P3HT and PCBM molecules are shown in Figure 3.2.

3.4 Preparation of P3HT, PCBM and P3HT:PCBM blend solutions

3.4.1 *Effect of Annealing Temperature*

The mass of P3HT and PCBM powder was measured using an electronic balance. Both P3HT and PCBM were diluted in 1ml chloroform or 1,2-dichlorobenzene which serves as an individual solvent or co-solvent. Then, the solution was vigorously stirred for 48 hours at room temperature to maximize mixing with concentration of 30 mg/ml. The solutions were deposited using spin coating technique at 3000 rpm for 30 s onto the substrates. For thermal treatment process, the sample was thermally treated using a hotplate for five minutes with temperature varies from 75°C to 175°C.

3.4.2 *Effect of Slow Formation of the Thin Layer*

For the second part, to study the effect of slow formation process on the thin film sample, the solution of P3HT:PCBM mixture were carried out by dissolving both materials in 1,2-dichlorobenzene solvent and stirred for 48 hours to achieve the optimum mixing. The concentration of the solution was set to 60mg/ml with 1:1 weight ratio of P3HT:PCBM. The photoactive layers of were prepared using three different

techniques. Pristine sample was prepared by spin-coated the mixed P3HT:PCBM solution onto the substrate using at 1500rpm for 60s, and no other further treatment was applied to the sample. The second sample was prepared similar to the first sample, but further thermal treatment was used by quickly annealed the sample after deposition, using a hot plate at temperature 125°C for 10 minutes. This second sample was labeled as thermal treated sample. After deposition onto the substrates, the last sample was quickly transferred into a Petri dish that filled with the saturated vapor of 1,2-dichlorobenzene and left for 20 minutes, slowing the formation of photoactive film. This last sample was then thermally annealed using a hotplate for 10min at 125°C and labeled as Slow-solvent-vapor-treatment sample.

3.4.3 Effect of Solvent on The properties of P3HT:PCBM Blend Film

For the third part, chloroform and 1,2-dichlorobenzene were used to studies the effect of using a mixture of solvent. The solution of P3HT:PCBM was prepared by mixing both materials and dissolved in solvent of 100% 1,2-dichlorobenzene (DCB) and also cosolvent consist 50% chloroform and 50% 1,2-dichlorobenzene (DCB:CH) and stirred for 48 hour to maximize mixing. The concentration of P3HT:PCBM was set to 60mg/ml with 1:1 weight ratio. The ‘slow-solvent-vapor-treatment’ process was utilized in the film formation method.

3.5 Substrate Cleaning

Glass substrates were used for morphology and optical studies and indium-tin oxide (ITO) coated glass is used for photovoltaic device preparation. The substrate needs to be cleaned appropriately to remove any contamination. The glass substrates were cleaned by immersing them in DECON™ foam solution and then placed in an ultrasonic bath for 16 minutes in order to shake off stubborn grease and dirt from the substrates' surface. Afterward, they were rinsed using deionised water, acetone solution, ethanol solution, and then rinsed again in the deionised water sequentially. Lastly, the glass substrates were dried using nitrogen gas. The procedure to clean the ITO substrate was slightly different. The substrates were immersed in ethanol:deionized water (4:6 ratio) and treated in ultrasonic bath for 16 minutes. Then the substrates were rinsed similar to that of the glass substrates.

3.6 Spin Coating Technique

Spin coating technique was used in this study to produce a uniform thin organic layer with a controlled thickness. This technique has been used for several decades to produce thin films and also been widely used in microelectronic industry to deposit a layer of photoresist film in the fabrication of integrated circuit (Petty, 2000). This process used a spinning motion in certain speed (around 1000-6000 rpm) to spread a small puddle of solution on top of a desired substrate. The solution will spread outward from the center and eventually off the edge of the substrate producing a thin layer on top of the substrate. The thickness and other properties of the film depend on the spinning rate, parameter chosen and also the nature of the solution.

The spin coating process is represented in Figure 3.2. The substrate was placed in the center of the spin coater plate and a vacuum pump was used to hold the substrate during spinning process. The prepared solution was then dropped on top of the substrate using a syringe and spread uniformly to fully cover the surface of the substrate. The spinning process was carried out resulting to a uniform thin layer coated on top of the substrate. The process was repeated for several times with a different set of solution to get the optimum condition. In general the higher the spin rate and the longer the spin time, the thinner the layer will be. The spinning rate chosen was around 1500-2000 rpm with maximum acceleration to ensure the spinning was starting at the require speed. The spinning time was around 30 second.

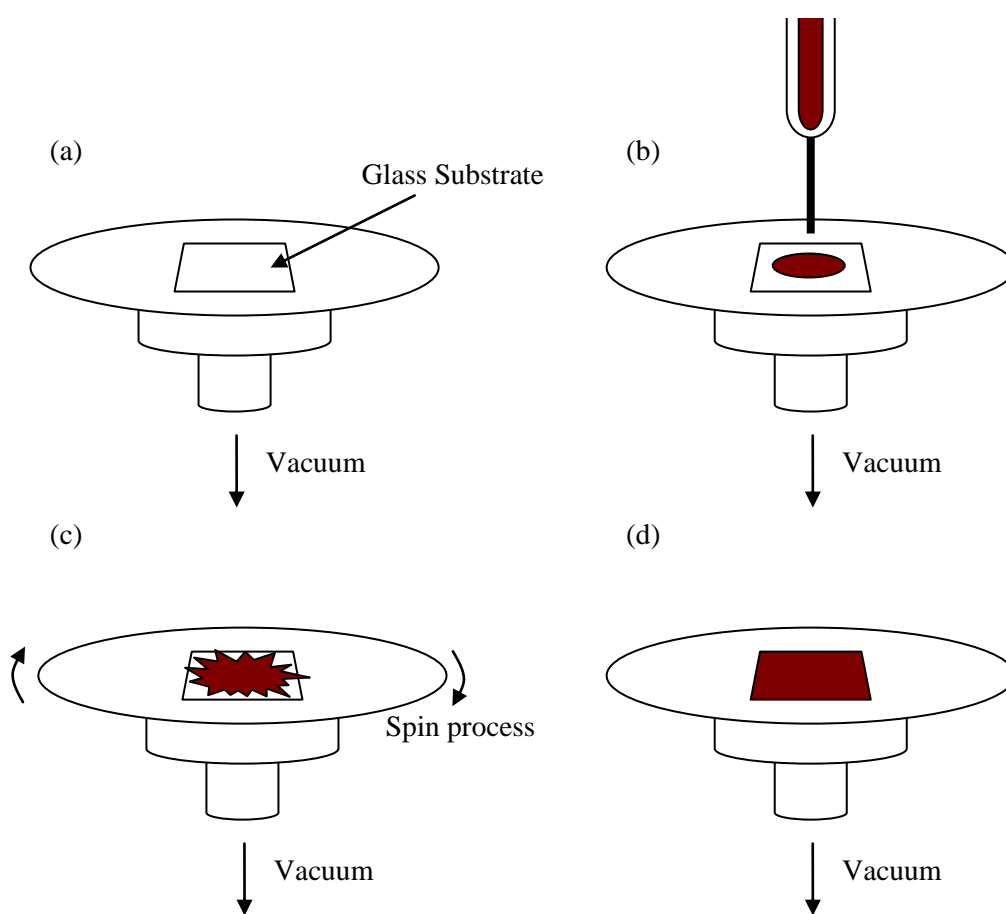


Figure 3.2: Schematic step by step of the spin coating technique

3.7 Aluminum Electrode Deposition

The aluminum electrode was deposited on top of the organic thin layer using a thermal evaporator. The schematic diagram of the thermal evaporator system that has been used is illustrated in Figure 3.4. The system was capable of pumping the pressure to 10^{-6} mbar. The system consist of glass vacuum chamber, two stage rotary pump, a diffusion pump, a penning gauge and two pirani gauges. The diffusion pump was cooled with flowing water for effective pumping. A base pressure of at least 10^{-5} mbar must be achieved before any deposition was carried out.

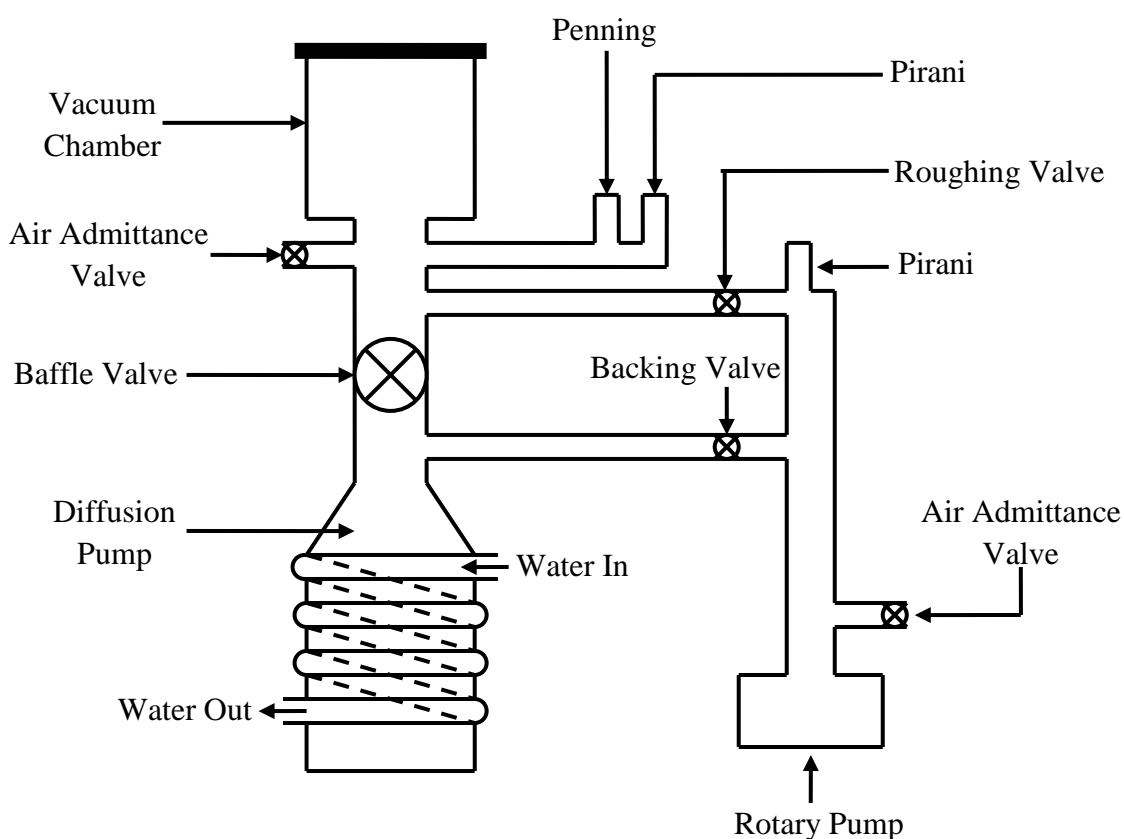


Figure 3.4: Schematic diagram of the thermal evaporation system.

Figure 3.5 shows the schematic of the vacuum chamber. The substrate was put on a aluminum mask with the desire electrode pattern. An aluminum wire that was going to be deposited is cut about 0.8 cm and hook to the tungsten wire. After the pressure inside the chamber achieved more than 10^{-5} mbar, a current was applied through the tungsten wire and increased slowly to about 40 A where evaporation took place. The aluminum eventually melted and evaporated inside the chamber and finally deposited on the sample that been placed on the upper side of the chamber. The shutter was close for a few minute after the aluminum started to melt and evaporate to obtain a good quality deposition. Electrical contact was made by using silver paste. The final device constructed is shown in Figure 3.1.

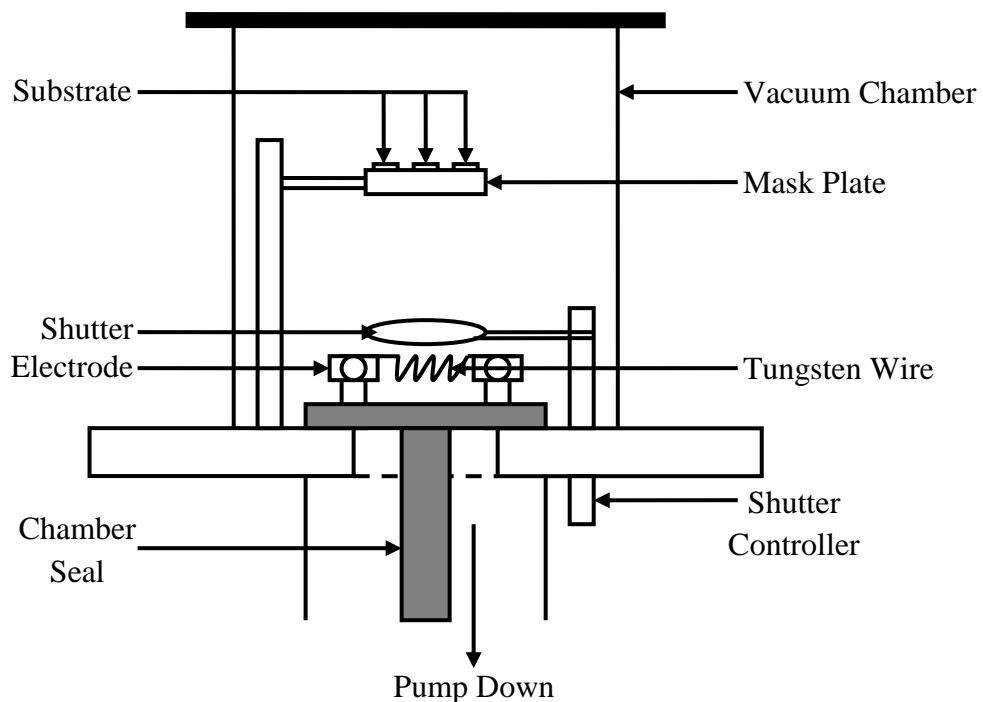


Figure 3.5: Vacuum chamber schematic diagram.

3.8 Thickness Measurement

The KLA Tencor P-6 profilometer is used to determine the thickness of the prepared organic thin films for this study. A contact profilometer is one of the instruments that have been used to measure the thickness of the thin films. This instrument uses a diamond stylus which moves laterally throughout the surface of the thin film. A scratched line was made on the surface of the film to create the difference height between the substrate and the surface of the film. Basically, it measures the thickness based on the difference height between the substrates and the thin films. The thickness of the thin film was measured from the steps height different between the substrate (base) and the thin film layer. In this work, the film was scratched at five different positions and the average value was taken as the thickness of the film.

3.9 Thin Film and Device Characterization

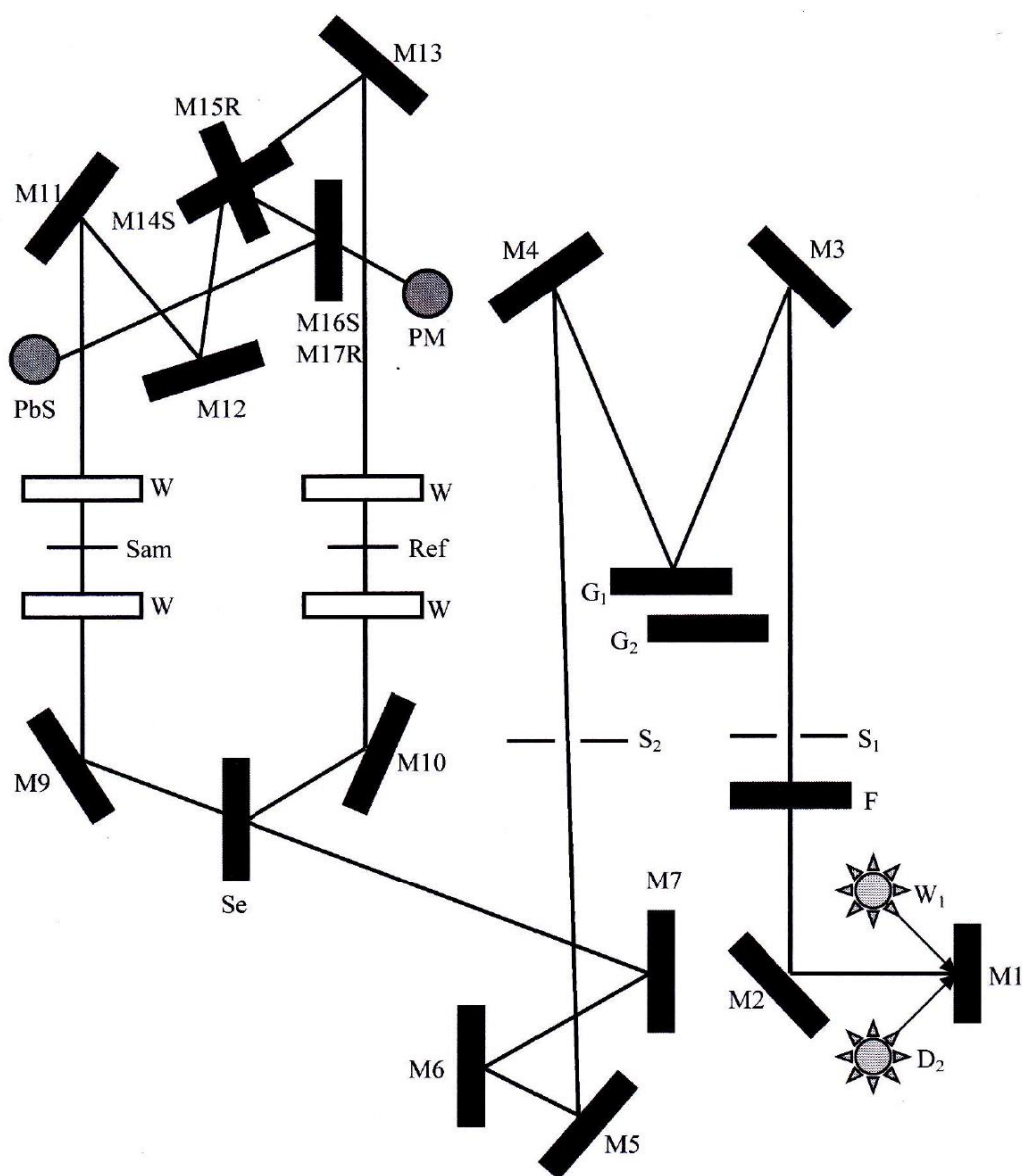
Absorption spectra measurements were carried out using Jasco V-570 UV/VIS/NIR spectrophotometer. Raman measurement was done using Jobin Yvon HR 800 UV at excitation wavelength of 512nm. A Siemens D5000 X-ray diffractometer was used to record the X-ray diffraction (XRD) patterns. Veeco D300 Atomic force microscopy is used to measure the samples surface roughness. Finally current-voltage (I-V) measurements were recorded using Keithley 236 source measure unit. The I-V characteristics of the photovoltaic devices were measured in the dark as well as under a white light illumination of a tungsten halogen lamp.

3.9.1 Ultraviolet – Visible-Near infrared Spectrophotometer.

In this work, to obtain the optical transmission spectrum of P3HT, PCBM and P3HT:PCBM blend thin film, the Ultra-violet Visible Near-infrared (Uv-Vis-Nir) Jasco model V-570 spectrophotometer was used. Figure 3.6 show the schematic diagram of the setup of the Uv-Vis-Nir spectrophotometer.

The UV spectrum region fall in the 100 to 400 nm, the visible spectrum fall from 400 to 700 nm and near infrared is 700 nm above (Figure 3.7). The UV-Vis-Nir Jasco spectrophotometer model V-570 measures the spectrum at a wavelength range from 250 to 2500 nm. A deuterium discharge tube with a wavelength range between 190 to 350 nm is used as a light source in the ultra-violet region and a tungsten iodine lamp with wavelength range between 340 to 2500 nm was used as a light source in visible to near infrared region. The light beam was converged before entering the monochromator. It was dispersed by a grating in the monochromator and the light passing through the exit slit was monochromated. This light was split into two light paths by a sector mirror, one incident on the sample to be measured and the other on the reference sample. Four different phenomenon occur when the light hit the sample namely absorption, transmission, reflection and scattering. The light that has passed through the sample or reference sample was then incident on the photomultiplier tube or Plumbum Sulfide (PbS) photoconductive cell (Xirochaki, 1998). The light from PbS photoconductive cell was converted into an electrical signal, which then was decoded into a digital form. The signal was processed and executed by software which will then be displayed as spectrum for the film. Light source change and wavelength trigger during the measurement process were controlled by operation software. In starting the measuring process, two reference glass substrates were placed in the sample holder for

scanning to produce the baseline for the transmission spectrum in the wavelength range of 250 to 2500nm. Then, one of the glass substrate was removed and replaced with the organic thin deposited on glass, while the other acts as a reference. The transmission spectrum of the sample was obtained within the same wavelength range.



W_1, D_2 : Light Source	M : Mirror
S : Slit	F : Filter
G : Grating	Se : Beam Splitter
PM : UV/VIS detector	PbS : NIR Detector
Sam : Sample	Ref : Reference

Figure 3.6: The schematic diagram of the components of a UV-Visible/NIR spectrophotometer.

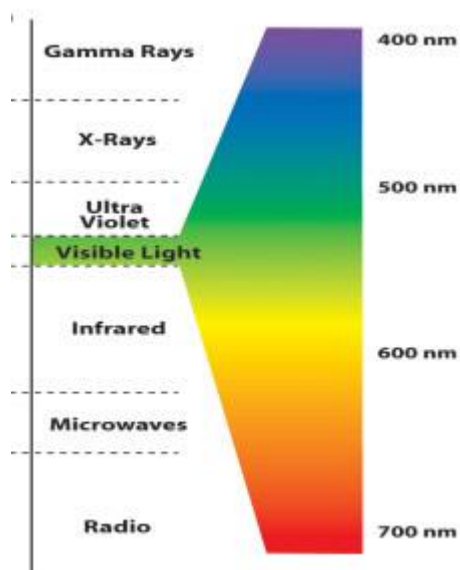


Figure 3.7: The visible spectrum with respect to infrared and ultraviolet radiation.

Ultraviolet-visible spectrophotometer is used in ultraviolet-visible spectroscopy to measure the intensity of light that passing through a sample (I), and compares it to the initial intensity of light before it passes through the sample (I_0). According to the Beer –Lambert Law, the measured absorbance, A is given as

$$A = -\log I / I_0 = -\log (\%T) \quad (\text{Equation 3.1})$$

where, the ratio I / I_0 is called the transmittance, and is usually expressed as a percentage (%T) (Mehta, 2012).

3.9.2 X-ray Diffraction Measurement.

Diffraction technique is a practical and powerful tool to study structure. The physical and chemical properties of a material are closely related to the structure of the material. The XRD measurement was used to determine the evidence of microcrystallinity in the P3HT:PCBM blend films prepared and the effect of using different preparation method. In this work, the X-Ray Diffractometer model SIEMENS D5000 was used to obtain the diffractogram of the P3HT:PCBM sample using a Cu-K α source ($\lambda=1.5402\text{\AA}$).

3.9.3 Atomic Force Microscopy.

Atomic force microscope (AFM) is a very high-resolution type of scanning probe microscope, which can result in a resolution of fractions of a nanometer, much better than the optical diffraction limit. Like all other scanning probe microscopes, the AFM utilizes a sharp probe which is a tip on the end of a cantilever that bends in response to the force between the tip and the sample, moving over the surface of a sample in a raster scan.

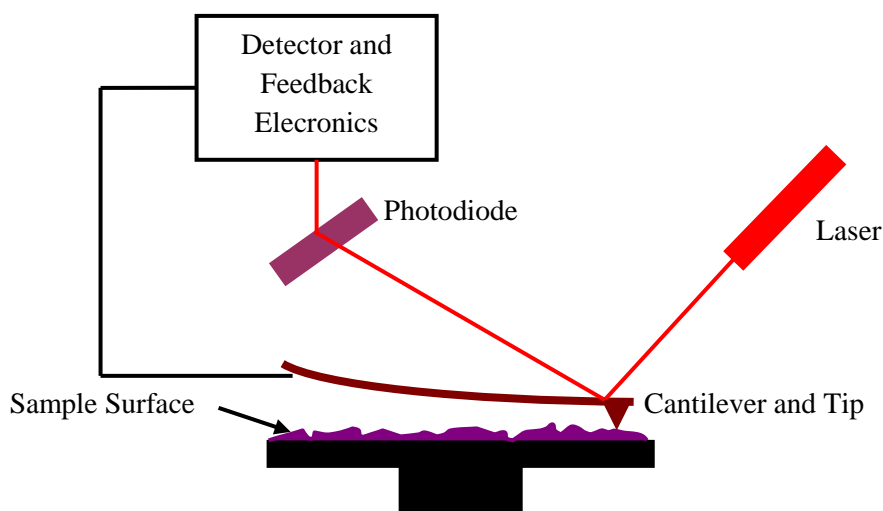


Figure 3.8: Block Diagram of Atomic Force Microscope

As shown in Figure 3.8, the AFM consists of a microscale cantilever with a sharp tip (probe) at its end that is used to scan the surface of sample. Usually, the cantilever is silicon or silicon nitride with a tip radius of curvature in the range of nanometers. When the tip approaches to a sample surface, the interaction forces that exists between the tip and the sample will cause the cantilever deflects. As long as the cantilever obeys the Hooke's law for small displacements, the interaction forces between the tip and the sample can be found. These forces may include Van der Waals forces, chemical bonding, electrostatic forces, mechanical contact force and so on. Besides these forces can be measured by AFM, some additional quantities may simultaneously be measured through the use of specialised types of probe. The measurement of deflection can be done using a laser spot reflected from the top of the cantilever into photodiodes. Typically, the sample is mounted on a piezoelectric tube. This piezoelectric tube enables to move the sample in the z direction for maintaining a constant force, and the x and y directions for scanning the sample.

AFM can be operated in two modes, which are with feedback control and without feedback control modes. If the electronic feedback is switched on (a feedback mechanism is carried out), the positioning piezoelectric tube enable to adjust the distance between the tip and the sample surface, by responding to any changes in forces which are detected. This can avoid the tip from getting too close to the sample surface until collides with it, causing damage. However, if the electronic feedback is switched off, then the microscope is said to be operating in constant height mode. This mode of operation is particularly useful for imaging very flat samples at high resolution ("Atomic force microscopy," 2012).

3.9.4 Raman Spectroscopy

The Raman measurement was done using Jobin Yvon HR 800 UV at excitation wavelength of 512nm to measure and obtain the Raman spectra of the samples. The samples were scanned from 200 cm^{-1} to 1000 cm^{-1} for the P3HT, PCBM and P3HT:PCBM films deposited on the glass substrate.

3.9.5 Current-Voltage Characteristic.

The photovoltaic behavior of the organic solar cell was investigated by a current-voltage measurement. From this measurement we will identified the open circuit voltage (V_{OC}) and the short circuit current (I_{SC}) of the cell. The open circuit voltage is defined as difference of electrical potential between two terminals of a device when there is no external load connected. In other word, the voltage across the device is measured with no external load but only the consequent internal load which is the resistant of the cell and its electrical interfaces.

The schematic setup for the I-V measurement is illustrated in Figure 3.9. The source of illumination was a Xenon Lamp, place in a Newport Universal Arc Lamp Housing 500 Watt Family model 67005. The arc lamp housing is powered by a Newport Arc Lamp Power Supply model 69907. An AM 1.5 filter is placed between the light source and the sample to get the standard AM 1.5 spectrum. The I-V curves were measured in the dark and also under the simulated sun radiation. The data was collected using a Keithley 236 source measuring unit connected to a computer. The signal was processed and executed by a Lab-view software to produce the I-V curve.

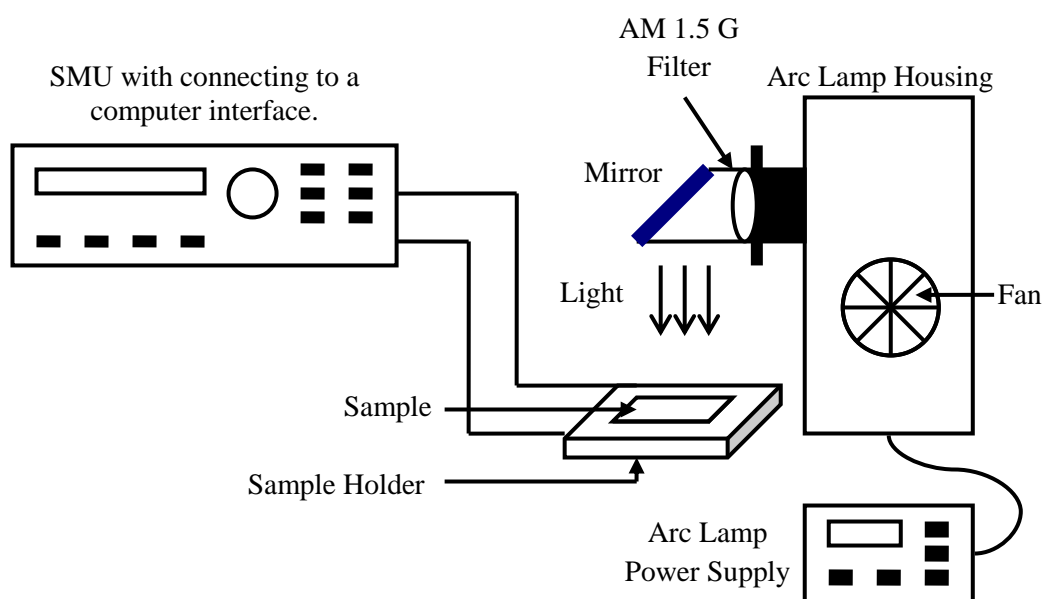


Figure 3.9: Schematic setup for the current-voltage measurement

To characterize an organic solar cell, we need to focus on the fourth quadrant of the current-voltage (I-V) curve. Referring to Figure 2.9, in the dark, the I-V curve shows a diode behavior where there is no current flowing in the cell until the voltage is higher than open-circuit voltage (V_{OC}), when current is flowing heavily at forward bias. When the cell is exposed to a light source, the I-V curve is shifted down by the short-circuit current (I_{SC}). The V_{OC} is the maximum voltage different achievable between the two electrodes, usually around 0.5-1.5V for organic cell, higher than inorganic cells. When the cell is placed on open-circuit condition and illuminated, electron flow to the low-workfunction and hole flow to the high-workfunction. At some point the charge build up to a maximum value same equal to the V_{OC} that is limited to by the different workfunction of the two electrode (Marks et al., 1994).

I_{SC} determined the maximum value that can run through the cell. This amount can be measure by connecting the two electrodes when the potential across the cell is set to zero and current flow is measure while the cell is illuminated. I_{SC} also gives the information about the charge separation and transport efficiency in the cells. The

magnitude of I_{SC} depends on the illumination power. For organic solar cell, for intensity of 100mW/cm^2 (AM1.5) will give around $0.20\text{-}80\text{mA/cm}^2$. The maximum work that the cell can give is when the product between the current, and the voltage, is the largest, current maximum (I_{\max}) and voltage maximum (V_{\max}). The quantum efficiency (QE) is the number of generated electrons per absorbed photon. The fill factor (FF) is given by:

$$FF = \frac{V_{\max} \cdot I_{\max}}{V_{OC} \cdot I_{SC}} \quad (\text{Equation 3.2})$$

And to determine the efficiency of a solar cell, this power is compared with the light intensity. The power conversion efficiency (PCE) is:

$$\eta_{POWER} = \frac{P_{OUT}}{P_{IN}} = \frac{I_{\max} \cdot V_{\max}}{P_{IN}} = \frac{FF \cdot I_{SC} \cdot V_{OC}}{P_{IN}} \quad (\text{Equation 3.3})$$

Chapter Four

RESULT AND DISCUSSION

Results and Discussion

4.1 Effect of Annealing Temperature

In this part, a thermal process has been performed on the P3HT:PCBM blend films at 75 °C, 100 °C, 125 °C and 150 °C. The influence of thermal annealing temperature on the UV-Vis absorption, photoluminescence and X-ray diffraction spectra were investigated on the prepared films at different temperatures. The main objective of this study is to obtain the optimum temperature in producing a good absorption properties as well as the highest semi-crystalline portion of the polymer in the blend film.

4.1.1 UV-Vis absorption measurement

Figure 4.1.1 shows the absorption spectra of P3HT:PCBM blend film for various annealing temperatures. The absorption of the blend films in the visible range between 450 nm to 650 nm with a peak at 478 nm, is ascribed to the π - π^* transition of the P3HT conjugated backbone system (Ge, 2009; Shrotriya et al., 2005; Xie et al., 2011). On the other hand, a small absorption band of the blend film appears in the UV region of 320 to 340 nm, corresponds to the absorption by PCBM molecules (Ge, 2009). There is slight rise in absorption coefficient upon annealing temperature, which can be due to the reduction in the sample thickness. It can be clearly seen from this figure, the peak wavelengths are red-shifted from 478 nm to 510 nm for the variation of pristine sample to the annealing temperature between 75 °C to 150 °C.

The absorption coefficient values of the peak together with the corresponding peak position at particular wavelength are tabulated in Table 4.1. From the analysis of

this red-shift feature, there is a change of 5% in the peak wavelength for the pristine blend sample to the annealed sample at 75 °C. From the table, it can be noted that a significant change upon annealing process occurs when the blend sample has been annealed at 100 °C with 18% red-shift of the wavelength peak. This red-shift indicates that the mean conjugate length of the P3HT has increased by improving the arrangement of the planar polymer chain as well as via formation of polymer crystallites in the annealed sample as a result of thermal annealing (Vanlaeke, Swinnen, et al., 2006). Nevertheless, the increment in the red-shift is no longer observed upon increasing the annealing temperature from 100 °C to 150 °C, with the peak stays at 510 nm.

Several attempts have been performed to obtain absorption spectrum of the annealed sample at 175 °C, but not succeeded. The annealing process of the P3HT:PCBM blend film (under ambient condition) at such high temperature has caused the sample to oxidize and degrade, which can be observed by naked-eyes; some part of the sample has been removed. Thus the optimum annealing temperature of 125 °C has produced a significant improvement in the polymer packing as well as the absorption coefficient. This temperature is used in the next parts of studies of photoluminescence and X-ray diffraction measurements.

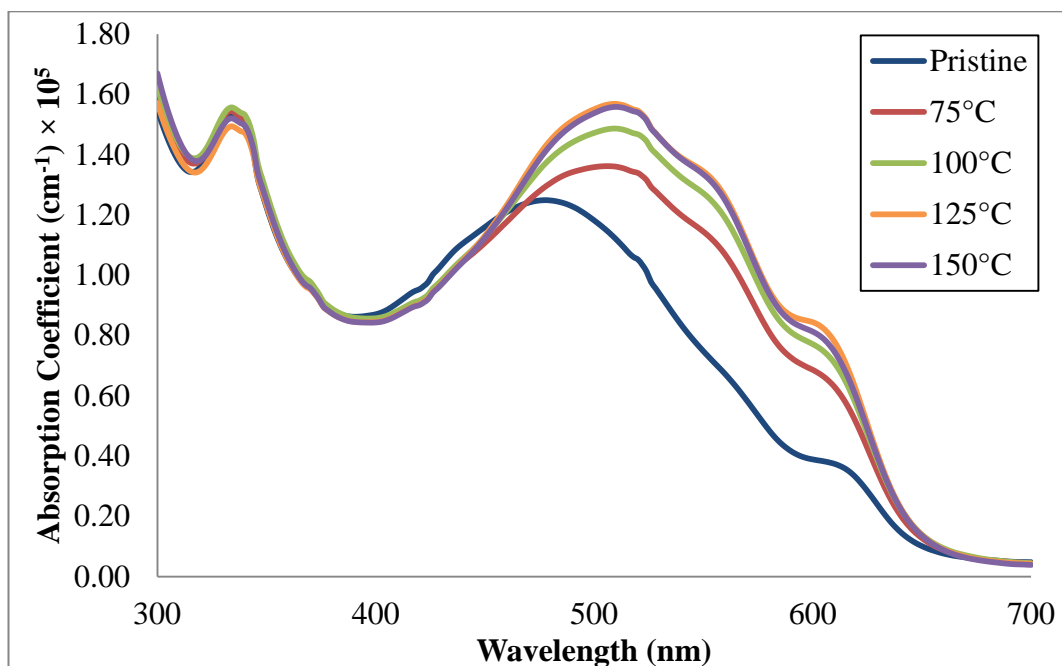


Figure 4.1.1: Absorption coefficient spectra of P3HT:PCBM blend film with different annealing temperature.

Table 4.1.1: Variation of absorption features with annealing temperature

Annealing temperature	Maximum absorption coefficient (cm^{-1}) $\times 10^5$	Peak wavelength (nm)	% red-shift of peak wavelength	Optical energy gap (eV)
Pristine	1.25	478	0	1.938
75	1.36	506	6	1.948
100	1.49	510	18	1.950
125	1.57	510	18	1.952
150	1.56	510	18	1.950

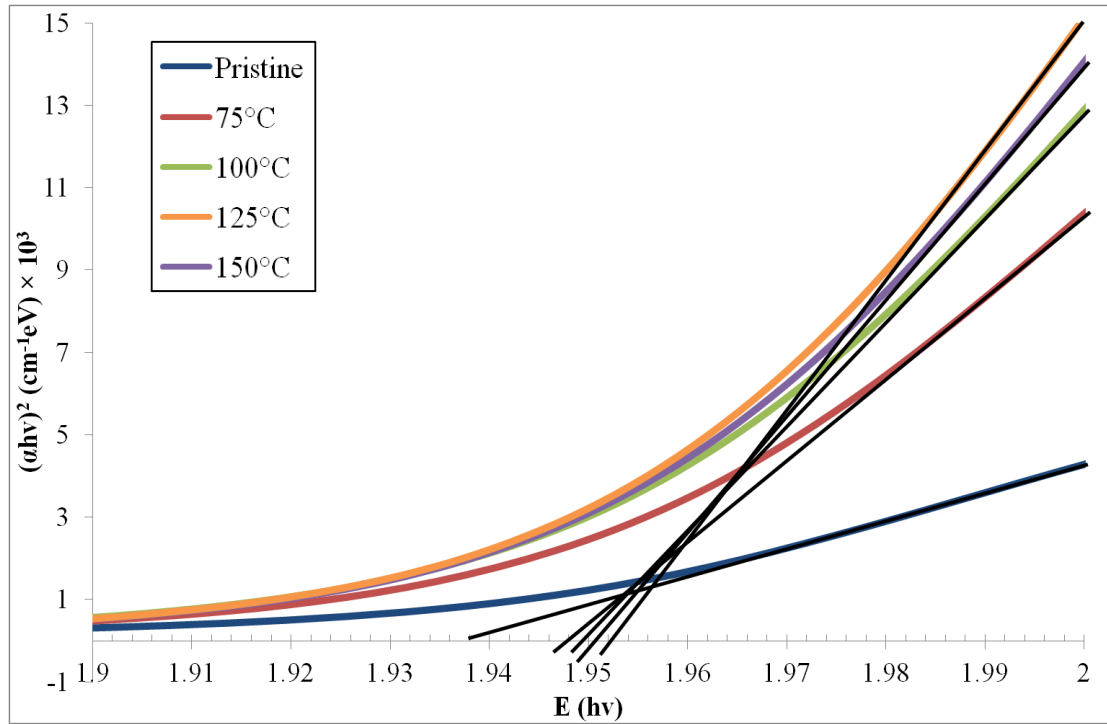


Figure 4.1.2: The plot of $(\alpha hv)^2$ vs hv of P3HT:PCBM P3HT:PCBM blend film with different annealing temperature

In general, Tauc's equation is used to estimate the band gap of inorganic materials (Tauc, 1986). Nevertheless this model has been utilized in many organic materials including the films used for organic solar cells (Muhammad et al., 2010). By utilizing the assumption from the Tauc model (Muhammad, et al., 2010; Tauc, 1968), where the absorption edge has a parabolic variation with photon energy (Dridi et al., 2009), it can be estimated the band gap equation is given by:

$$\alpha hv = \alpha_0 (hv - E_g)^n \quad (\text{Equation 4.1})$$

where α_0 is the energy independent constant, n is the exponential value.

Value of n depend on the type of transition in which $n = 1/2$ for direct transition, $n = 2$ for indirect allowed transition and $n = 3/2$ for forbidden transition (El-Nahass et al., 2003). If P3HT:PCBM is considered to have a direct absorption coefficient type (Muhammad, et al., 2010; Muhammad et al., 2011) and by applying equation 4.1,

$(\alpha h\nu)^2$ versus $h\nu$ can be plotted to identify the energy gap of the samples as shown in Figure 4.1.2. Extrapolating the straight line of tangent of the curves to $h\nu = 0$, give the value of the optical energy gap. This optical energy gaps for the pristine, annealed at 75 °C, 100 °C, 125 °C and 150 °C samples have been estimated to be 1.938 eV, 1.948 eV, 1.950 eV, 1.952 eV and 1.950 eV, respectively. This results of increment in optical energy gap in P3HT:PCBM blend films upon annealing temperature has also been observed by other researchers (Ge, 2009). However, in some cases, the optical energy gaps has been lowered by applying heat to the samples (Xiaoyin et al., 2010).

The overall results are listed in Table 4.1. From all the collected data and after analyzing the value of energy gap of all of the samples it can be observed that by exposing the sample to the thermal treatment under ambient condition, the energy gap has increased. Thus, this annealing process is not a proper method in reducing the optical energy gap the P3HT:PCBM blend films. The reduction in energy gap is one of the crucial factors to obtain a good performance in the polymeric solar cells; in which the many photons can be absorbed in the active layer to generate charge carriers (Petritsch, 2000; Sun et al., 2005).

4.1.2 Photoluminescence (PL) Spectra

In general, PL intensity of a pristine thin film (either organic or inorganic) increases upon annealing. Thus, in this study, pure films of P3HT and PCBM are investigated, then the respective pristine film of the P3HT:PCBM blend is compared to the thermally treated film at the optimum annealing temperature of 125 °C. Figure 4.1.3 shows the PL spectra of P3HT, PCBM and the P3HT:PCBM blend films. The PL of pristine P3HT:PCBM blend is drastically quenched as compared to the pure P3HT film. This PL quenching indicates the photoinduced charge transfer in the blend sample becomes more efficient upon introducing PCBM into P3HT. This PL quenching phenomenon P3HT:PCBM blend is in agreement with other reported results of similar blends (H. Kim et al., 2006).

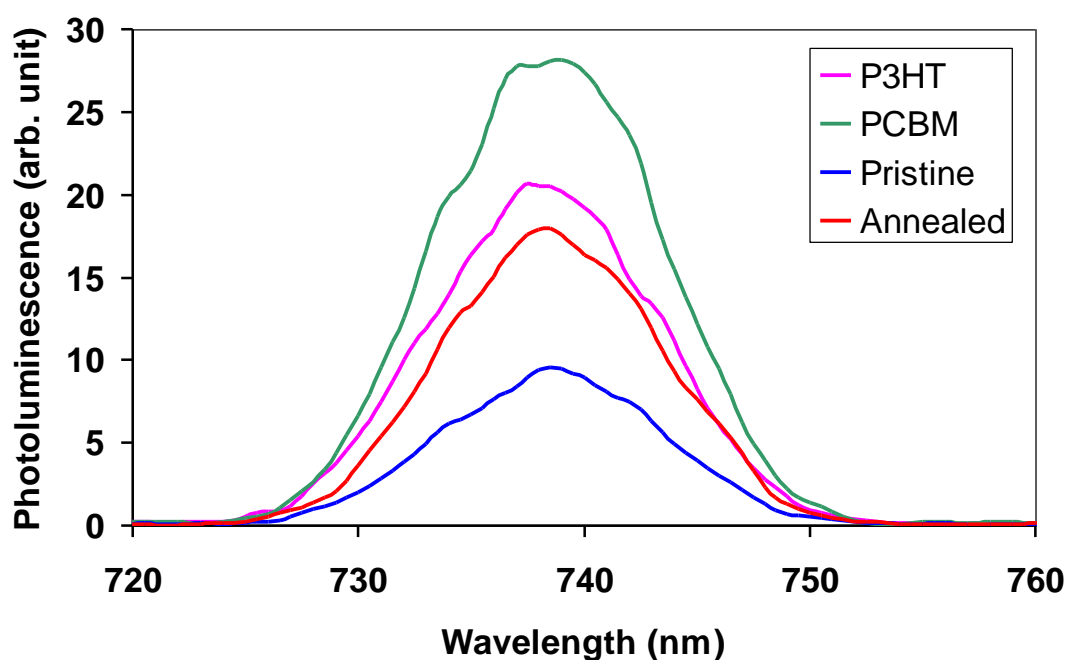


Figure 4.1.3: Photoluminescence spectra of P3HT, PCBM, pristine blend and annealed sample at 125 °C

4.1.3 X-ray Diffraction Spectra

Figure 4.1.4 shows the XRD spectra of P3HT and P3HT:PCBM blend films before and after annealing at 125 °C. Most parts of the films are amorphous as indicated by the broad XRD features with only a small peak. Peaks at approximately 2θ of 5.4° appear in all diffractograms.

The XRD intensity of the P3HT:PCBM blend films is reduced by 40% relative to P3HT alone. The spectrum of P3HT shows the present of the partially crystalline phase, embedded within a large portion of amorphous phase. But upon thermal annealing at the blend films, the intensity is increased by 54% relative to the pristine intensity value. Furthermore, the XRD peak of the annealed sample has become narrower and more intense, indicating of an improved coherent scattering of the X-rays due to larger crystalline domains. This quite significant increment in XRD intensity may be attributed to the larger portion of crystallite phase embedded within the amorphous phase.

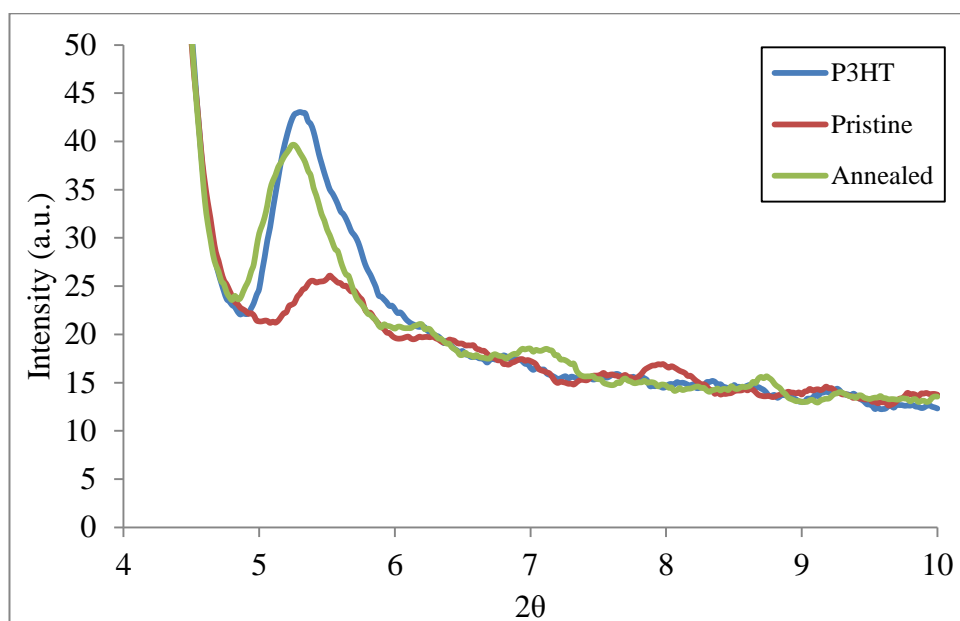


Figure 4.1.4: X-ray Diffraction spectra of P3HT, pristine blend film and annealed sample at 125 °C.

Table 4.1.2: Variation in the interplanar distance and the crystalline thickness for the P3HT, Pristine and Annealed samples.

Solvent Type	P3HT	Pristine	Annealed (125 °C)
2θ (°)	5.28	5.45	5.18
FWHM (B) (rad)	0.00906	0.00977	0.00733
Interplanar Distance (d-spacing) (nm)	1.67	1.62	1.64
Crystalline Thickness (nm)	16.02	14.85	19.79

Using the Scherrer's equation, the estimated crystalline size of the sample can be calculated. Scherrer's equation is given by:

$$L = \frac{K\lambda}{B \cos \theta} \quad (\text{Equation 4.2})$$

where L is the crystalline thickness, K is the shape factor which (0.94), λ is the source wavelength (0.1542 nm), and B is the full width at half maximum (FWHM) of the peak.

Annealing shifted the diffraction peak slightly to a lower 2θ angle. Using the Bragg's equation, the interplanar distance (d-spacing) was calculated. The interplanar distance is reduced when PCBM is introduced to the P3HT sample but this characteristic has tremendously increased when the sample has been thermally treated. The annealed blend sample has an interplanar distance of 1.64 nm compared to 1.62 nm for the pristine blend film. The crystalline thickness of the P3HT sample which is 16.02 nm has been decreased to 14.85 nm after PCBM was mixed. This result show that by introducing PCBM in the P3HT film to form blend of P3HT:PCBM, the crystalline portion has been reduced and this observation also has been reported by other researcher (Vanlaeke, Vanhoyland, et al., 2006). This could be due to the amorphous feature of PCBM molecules.

A good influence of the annealing process can be observed in the annealed blend film. The thickness of crystallite size for the annealed sample increased to 19.79 nm as compared to the pristine blend sample of only 14.85 nm. An increment by 30% of crystallite size is really a noteworthy effect on the formation of the P3HT:PCBM film upon a thermal treatment. This XRD result is strongly supported by the observation from the previous absorption spectra; as the blend sample has been increased in the molecular order of the polymer chain arrangement upon annealing

process. The polymer chain re-arrangement upon annealing has tremendously affected the molecular packing, hence enhances the crystalline portion of the polymer within amorphous film. This results are in good agreement with the reported observation(Vanlaeke, Swinnen, et al., 2006)

4.1.4 Summary

As a summary, thermal annealing process on the PCBM blend films at 75 °C, 100 °C, 125 °C and 150 °C. The absorption spectra of the films has shown a significant red-shift upon annealing, indicating the improvement of polymer packing due to the re-arrangement of the polymer chain. This absorption spectra result is further supported by the increment in the crystallite size of the polymer as indicated by the XRD spectra. The optimum temperature of 125 °C that obtained from the absorption spectroscopy measurement was used in the preparation of the fast grown film in next section of 4.2.

4.2 Effect of Slow Formation of the Thin Layer

In this part, three types of film formation processes were used to obtain a good P3HT:PCBM blend film, namely;

- (a) As deposited: the pristine blend film was characterized without any treatment,
- (b) Fast grown: the blend film was quickly annealed at 125 °C (this optimum temperature obtained from the study in part 4.1),
- (c) Slow grown: the blend film was exposed to solvent vapor for 20 minutes, then annealed at 125 °C.

4.2.1 UV-Vis absorption measurement

Figure 4.2.1 demonstrates the absorption spectra of P3HT:PCBM blend film ‘as deposited’, ‘fast grown’ and ‘slow grown’. The absorption for P3HT is visible between 400 to 650 nm, however below 400 nm, the absorption for PCBM is dominant. As discussed in chapter 4.1.1, the absorption of the fast grown sample (annealed) is higher than the pristine as deposited P3HT:PCBM blend sample. By applying heat to the sample, the ordering of the P3HT phase in the sample is improved and therefore increasing the absorption value of the thin film favorably in the range of 400nm to 650nm (see absorption of the fast grown). Besides, it can be seen from the fast grown spectrum, that the appearances of the two shoulders at 550nm and 610nm become clearer. The appearance of shoulders in the spectrum is well known as the indication of the ordering of P3HT molecules (T. A. Chen et al., 1995) and this will be further discussed and confirmed by the XRD result.

The absorption is further increased by slowing the formation of the film before the sample is heated. As evident in the slow grown process UV-Vis spectrum, the intensity of the peaks approximately at 470 to 530 nm, representing the intrinsic π - π^* transition of P3HT, substantially increase, leading to a rise in the absorption spectrum at the red part of the film. The results indicate that the gradual evaporation of the from the blend film in the slow grown sample causing a formation of a better reorganization of the polymer chains (Al-Ibrahim, et al., 2005; T. A. Chen, et al., 1995).

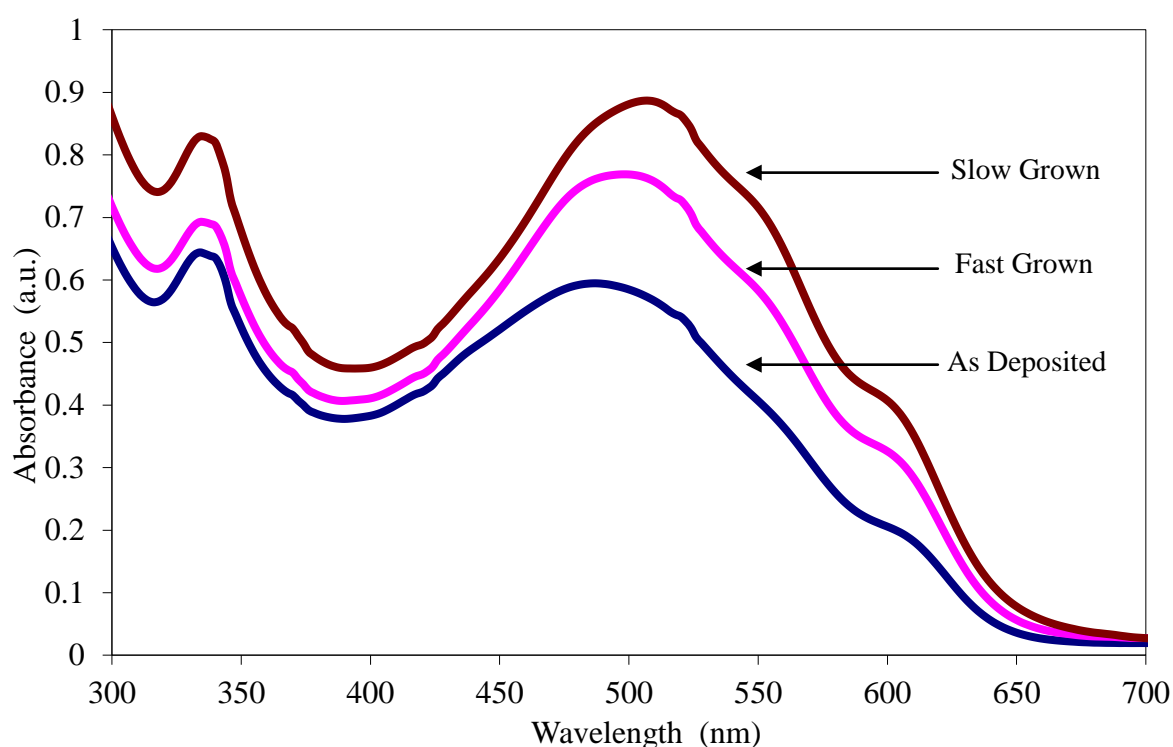


Figure 4.2.1: UV-vis absorption spectra of P3HT:PCBM blend film

The shoulder at 610 nm is associated with the interchain interaction (P. J. Brown et al., 2003; Chirvase et al., 2004). This shoulder intensity depends on the order degree in the intermolecular chains of the microcrystalline domains. Therefore, the increased intensity in the peak at 610 nm implies a higher level of molecular ordering (Guo et al., 2008). These optical changes will give rise to the solar cell efficiencies.

Thus, such process may create higher crystallinity due to a better ordering within the photoactive film and this will be discussed in the following section.

4.2.2 X-ray Diffraction Spectra

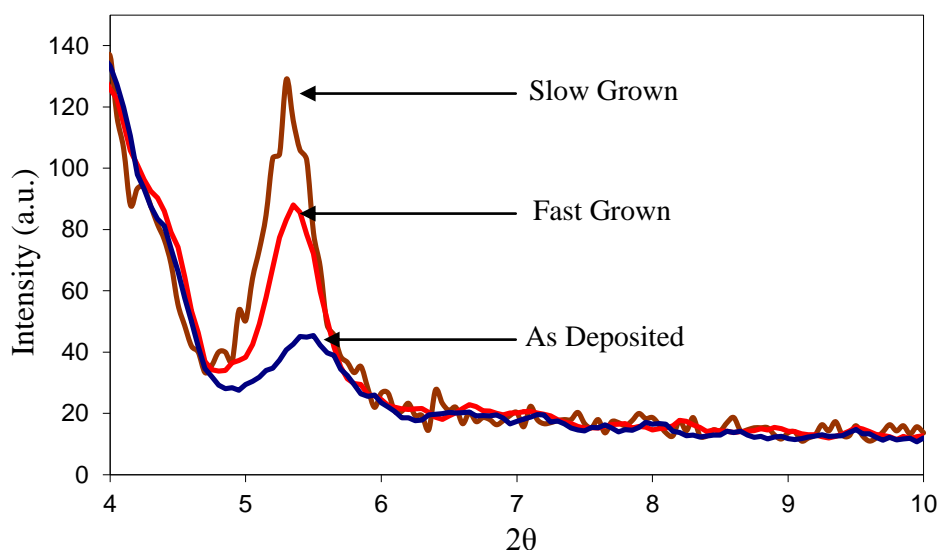


Figure 4.2.2: X-ray Diffraction of P3HT:PCBM blend film.

Figure 4.2.2 shows the XRD spectra for the first-order reflection of P3HT:PCBM blend films which is normally observed (T. A. Chen, et al., 1995; Erb et al., 2005; Vanlaeke, Swinnen, et al., 2006; Vanlaeke, Vanhoyland, et al., 2006; Zhokhavets et al., 2006). The blend films show there are present of crystalline phase. The XRD peak at approximately 2θ of 5.4° appears in the diffractogram attributed to the partial crystallinity of the P3HT crystallites which are dispersed in amorphous PCBM matrix. As known, by introducing PCBM molecules in the blend film, the crystallinity of P3HT polymer will drastically drop (Yang, et al., 2005).

The addition of PCBM is disturbing the formation of P3HT crystalline domains. The lowest peak was observed for the pristine of as deposited film. Upon annealing process of the fast grown film, the P3HT peak within the mixture film is drastically increased as previously discussed in part 4.1.3. Besides, the value of full width at half maximum (FWHM) has decreases representing the increase in the degree of crystallization and the grain size of P3HT domain.

By using Scherrer's formula of equation 4.2 (as previously discussed in section 4.1), the thickness of the crystallite can be calculated. The thickness of crystallite size as the fast grown sample has increased 20% as compared to the untreated of as deposited sample. Further improvement in crystallization has been achieved by means of the slow grown method. The peak from the slow grown film shift toward the lower angle compared to both of peaks from as deposited and fast grown film. The interchain spacing associated with the interdigitated alkyl chains in P3HT is also changed to 1.67 nm. The thickness of crystallite size has enhanced from 19.67 to 22.50 nm upon slowing down the process of film formation via exposing the blend film to the solvent vapor. This steady condition of the slow grown film method has promoted the formation of an organize P3HT within a uniform PCBM, which is consistent with well-define bulk heterojunction organized on the nano-to-micro level in the blend film (Guo, et al., 2008). The results of XRD are in agreement with the absorption spectra; the crystallinity and the ordering of the slow grown polymer can be improved via slow evaporation of solvent followed by thermal annealing process. The summary of the interplanar distance and the crystalline thickness for all three samples is tabulated in Table 4.2.

Table 4.2: Summary of the interplanar distance and the crystalline thickness for the as deposited, fast grown and slow grown film sample.

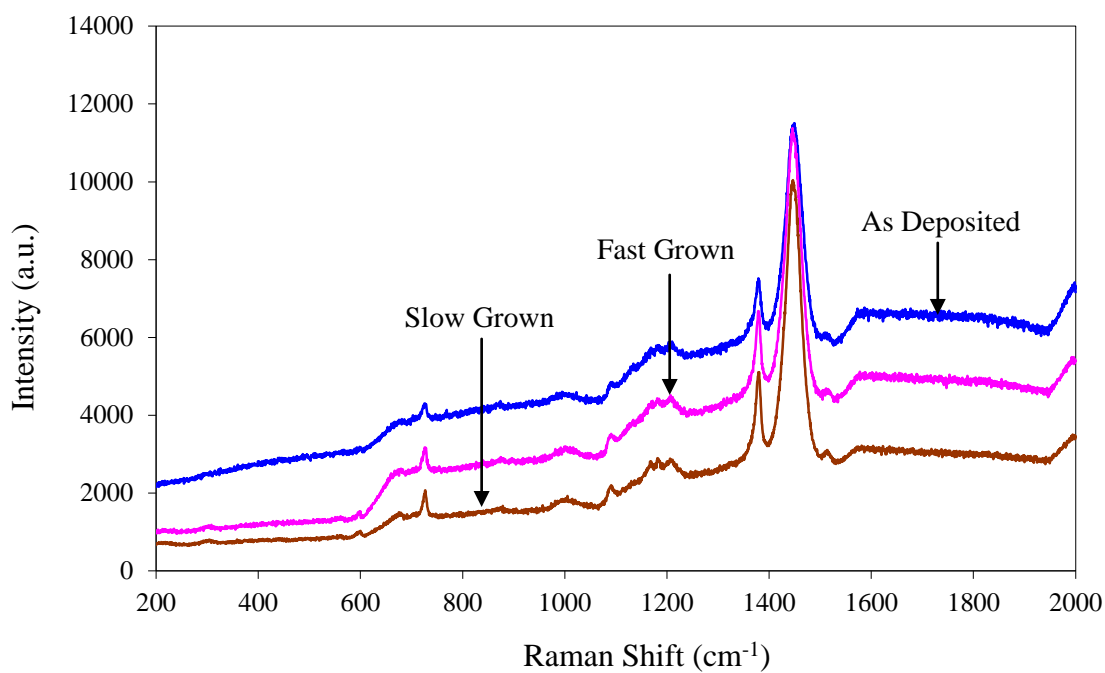
	As deposited	Fast grown	Slow grown
2 θ ($^{\circ}$)	5.45	5.40	5.30
FWHM (B)	0.00873	0.00698	0.00610
Interplanar Distance (d-spacing) (nm)	1.62	1.64	1.67
Crystalline Thickness (nm)	15.72	19.67	22.50

4.2.3 Raman measurement

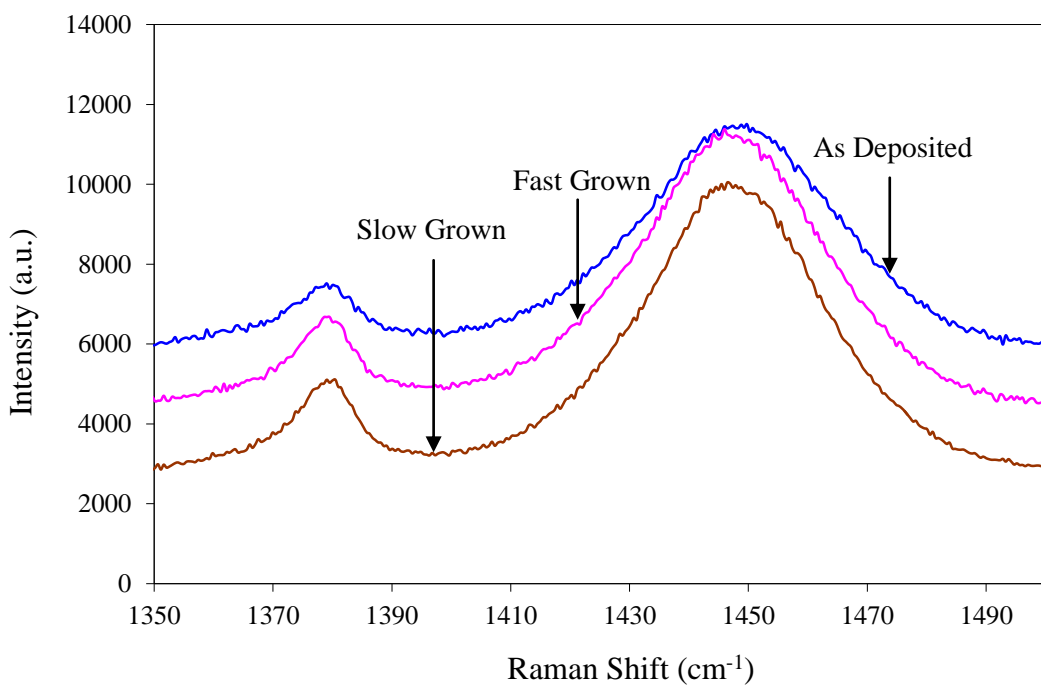
Raman spectra of all the three samples in the range 200 – 2000 cm^{-1} are shown in Figure 4.2.3(a). There are a few Raman peaks can be observed; the peaks on 715 cm^{-1} , 1380 cm^{-1} and 1440 cm^{-1} are assigned to the C-S-C, C-C and C=C respectively stretching deformation in the aromatic thiophene ring of P3HT (P. J. Brown, et al., 2003; Klimov et al., 2006; Louarn et al., 1996). The existence of PCBM molecules in the P3HT film did not contribute to the Raman modes of the P3HT:PCBM blend film (Heller et al., 1995).

In order to compare the effect of the three different methods of as deposited, fast grown and slow grown, focus is given on the region between 1350 cm^{-1} and 1500 cm^{-1} as shown on Figure 4.2.3(b), enlarged from Figure 4.2.3(a). There is indication of Raman shift at the C=C peak where it is shifted to a lower wavenumber (cm^{-1}), which is 1449.27, 1448.32 and 1446.90 corresponding to sample as deposited, fast grown and slow grown respectively. This downward shift in the wavenumber indicates that there is an increase in the crystallinity of the P3HT polymer and improvement of the effective conjugation length along the polymer back bone (Klein et al., 1975). Therefore, polymer film prepared by the slow grown method is more favorable with the

improvement of morphology for the transport charge carriers. There is also an interesting effect on the full width at half maximum (FWHM) of the peak can be observed. The peak becomes narrower and the FWHM of the fast grown sample is decreased significantly compared to the as deposited sample with the value of 34.21 cm^{-1} for fast grown and 34.58 cm^{-1} for as deposited sample. The use of slow grown method on the sample shows more improved state on the film. A narrower peak can be detected and the FWHM is decreased dramatically compared to the other two samples with the value of 32.78 cm^{-1} . Since the Gaussian widths of the Raman lines in heterogeneous systems are measure of their disorder (Mihailetchi et al., 2006), we can infer that slowing the film formation process reduces the disorder in P3HT-PCBM, consistent with packing arrangement of P3HT polymer segment as discussed previously in the XRD results. This correlation between the formation of higher crystallinity via thermal annealing and slow solvent evaporation has been further proven by the results of Raman spectroscopy.



(a)



(b)

Figure 4.2.3: Influence of film formation types on Raman spectra of P3HT:PCBM blend films, (a) Raman shift from 200 to 2000 cm⁻¹ (b) enlarged Raman shift from 1350 to 1490 cm⁻¹.

4.2.4 Atomic Force Microscopy

Figure 4.2.4 shows the atomic force microscopy (AFM) images in two dimensional as well as three dimensional of the as deposited, fast grown and slow grown thin films. It shows that when the sample has been thermally treated (see Figure 4.2.4(b)), the roughness of the sample is increased, suggesting the formation of the inter-penetrating P3HT:PCBM molecular network. According to previous researchers, this trend in the composite films seems to be due to self-organization of each P3HT and PCBM component through thermal treatment (Erb, et al., 2005; Mihailetschi, et al., 2006). The roughness for the slow grown (Figure 4.2.4(c)) is slightly higher than fast grown sample. The roughness is considered to be signature of P3HT polymer self-organize into more ordered structure through vapor treatment (Yang, et al., 2005). Slowing the evaporation process of the solvent solution form a better organize P3HT network in the film. The roughness of the as deposited, fast grown and slow grown sample is 5.146, 11.072 and 14.706 nm respectively. The AFM results are in agreement with the ordering arrangement of polymer chains indicated by the absorption spectra.

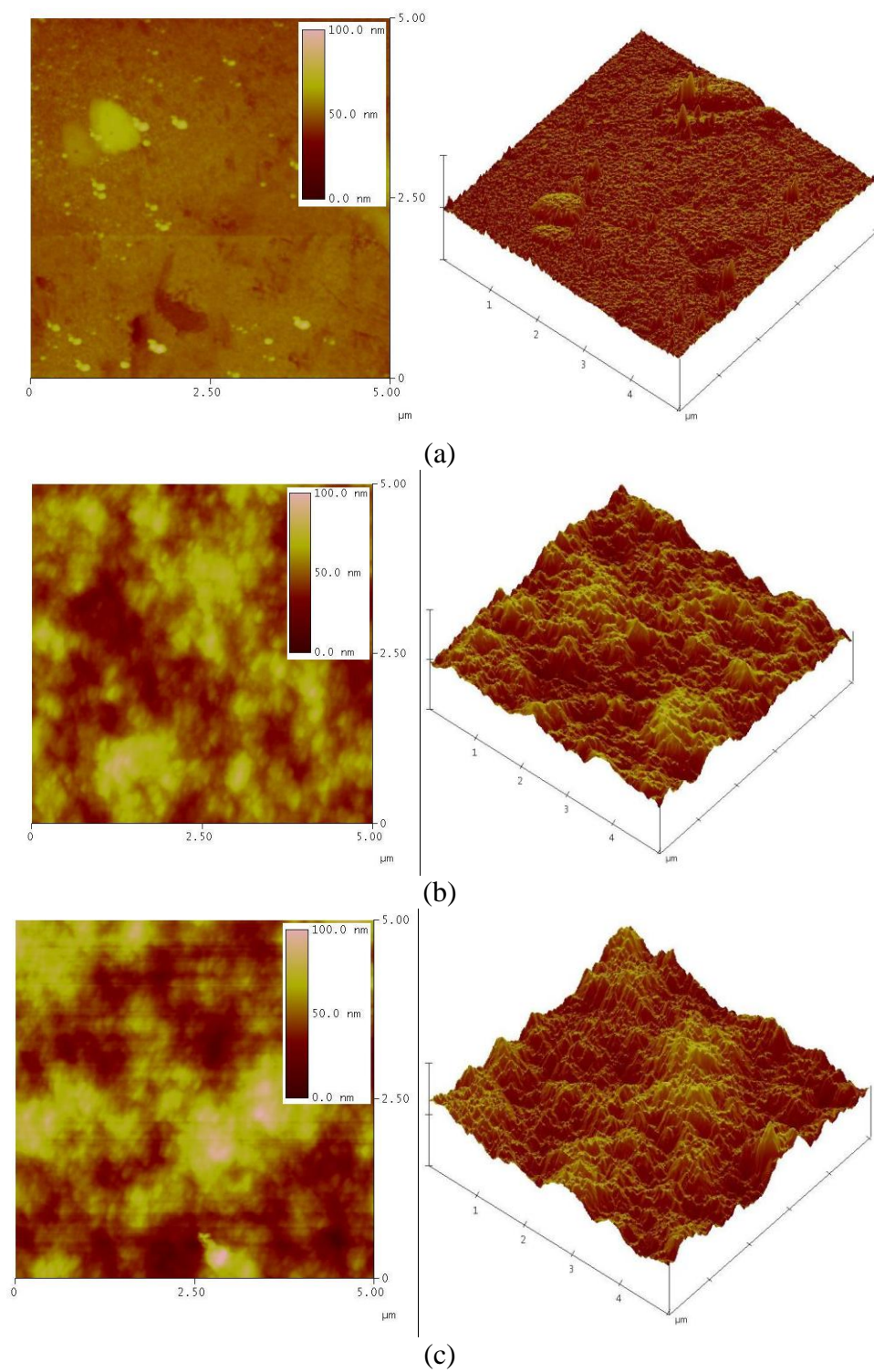


Figure 4.2.4: 2D and 3D atomic force microscopy images of (a) As Deposited, (b) Fast Grown and (c) Slow Grown sample.

4.2.5 J-V Characteristic

The current density-voltage (J-V) characteristic of the P3HT:PCBM solar cell is presented in Figure 4.2.5 . The open circuit voltage (V_{OC}) of the devices is around 0.3 to 0.5 V. The short circuit current for the annealed devices increase compared to the not annealed device. J_{sc} of the pristine as deposited P3HT:PCBM film has improved more than 20 times and 4 times compared to that of fast grown and slow grown sample respectively. The charge carrier mobility is strongly dependent on the crystallinity feature of the blend. Since the slow grown P3HT:PCBM blend film has produced a better feature of crystallite size as well as better polymer chain ordering, hence the performance of electrical properties of J-V characteristics are enhanced.

Thermal annealing improves the ordering of the film, so in principle, the charge carrier mobility is improved and so it reduces the recombination losses. Slowing the formation of the thin film further more increase the ordering. We can conclude that morphology modification as shown in the AFM images after thermal annealing and slowing the formation process improved the transport properties and therefore to reduction of recombination losses.

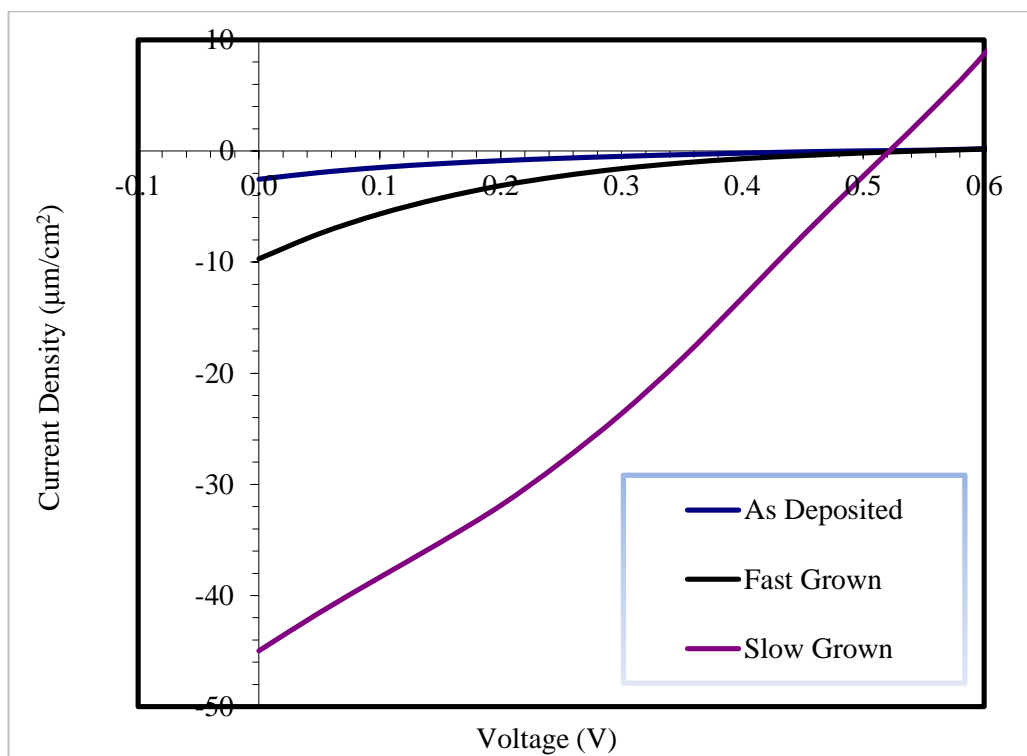


Figure 4.2.5: J-V plots for P3HT:PCBM solar cells prepared As Deposited, Fast Grown and Slow Grown.

4.2.6 Summary

As a summary, the difference processes in the film formation namely as deposited, fast grown and slow grown has been investigated on the P3HT:PCBM system. The XRD and Raman spectra have provided proofs of better crystallinity as well as a higher level of molecular ordering in the blend of the slow grown compared to the fast grown. Hence, the improvements in the photovoltaic characteristic of short-circuit current and open circuit voltage can be co-related to the enhancement in semi-crystallite size of the polymer blend.

4.3 Effect of Solvent on the properties of P3HT:PCBM Blend Film and Photovoltaic devices

In this part, three types of solvents were used in preparing the P3HT:PCBM blend film, namely pure o-dichlorobenzene (DCB), pure chloroform (CH) and o-dichlorobenzene:chloroform (DCB:CH) co-solvent. The influence of the three different types of solvents was investigated on the between the absorption coefficient, energy gap, crystallite size, surface roughness as well as photovoltaic characteristics of the P3HT:PCBM blend films.

4.3.1 UV-Vis absorption measurement

The comparison between the absorption spectra of the P3HT:PCBM blend prepared from pure o-dichlorobenzene (DCB), pure chloroform (CH) and o-dichlorobenzene:chloroform (DCB:CH) co-solvent is shown in Figure 4.3.1. It can be clearly seen that the blend film dissolved in DCB:CH co-solvent not only shows the highest value of absorption coefficient, but has the ability to broaden the absorption range which span most of the visible wavelength range from 450 nm to 650 nm compared to that of 100% DCB and 100% chloroform solvent. This indicates that a large number of photons are absorbed for using the mixture film prepared from DCB:CH co-solvent. Besides, for the film prepared in co-solvent, the peak is red-shifted to 514 nm, with an increase of about 4.9% and 7.5% compared to that of pure DCB and pure chloroform, which has the peak at 490 nm and 478 nm relatively. This result indicates that an increase of conjugation length of the polymer chains. Besides, the two shoulders in the absorption at 550 nm and 600 nm are well resolved for the film prepared from the co-solvent. This clear appearance of shoulders is an indication of better ordering of P3HT molecules, as discussed earlier (T. A. Chen, et al., 1995).

The formation of the photoactive film by using DCB:CH co-solvent is strongly influenced by the solubility of the blend component of P3HT:PCBM. A mixture of solvent DCB:CH yields better solubility than the pure single solvent. In fact, a uniform photoactive layer on the substrate (as observed by naked eyes) cannot be obtained from a blended solution of P3HT:PCBM in pure DCB solvent. This is attributed to its large surface tension that may lead to an occurrence of significant shrinkage upon the film, and thus affect the physical properties of the film itself. Furthermore, the film takes longer time to dry after the spin-coating process, due to such a much high boiling point of DCB (180.5 °C) compared to a lower boiling point of chloroform (62.2 °C). Thus, the addition of a moderate amount of chloroform into DCB has reduced the surface tension (Kawano et al., 2009). Moreover, a more film has been produced from the solvent mixture, and it takes an ample shorter time to dry under ambient condition. Therefore, the use of co-solvent in the P3HT:PCBM film preparation, allows the polymer to reorganize the polymer chains and forming a better film with good light absorption properties.

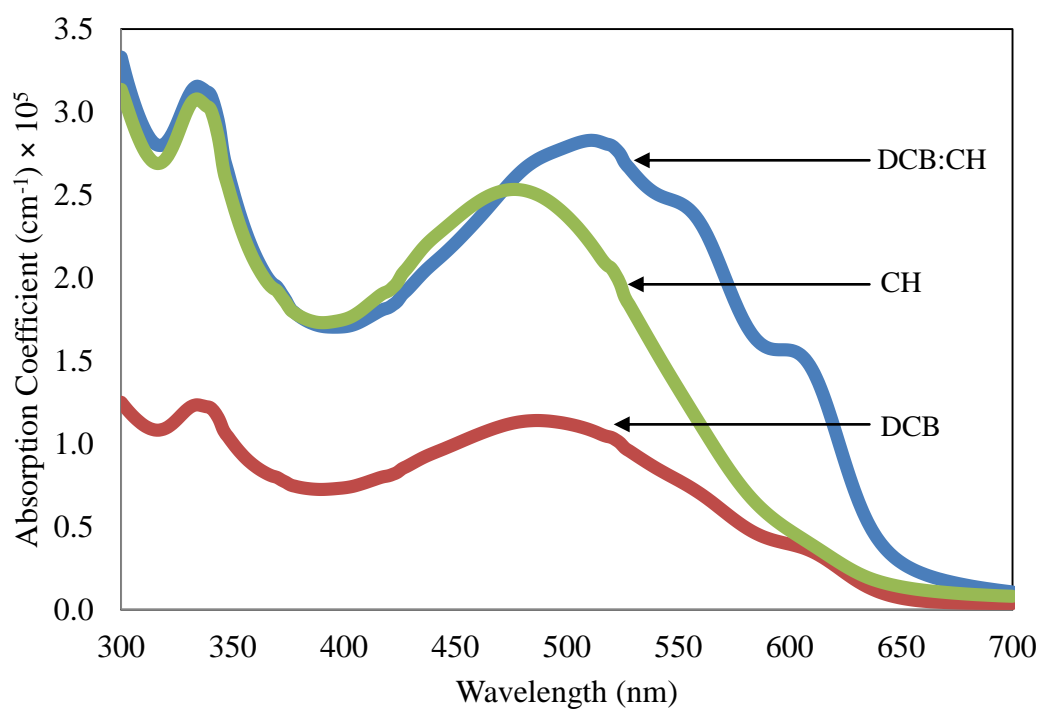


Figure 4.3.1: Absorption coefficient spectra of P3HT:PCBM blend films which were dissolved in pure DCB solvent, pure CH solvent and DCB:CH co-solvent.

Table 4.3.1: Variation of absorption with annealing temperature

Type of solvent	Maximum absorption coefficient (cm^{-1}) $\times 10^5$	Peak wavelength (nm)	Optical energy gap (eV)
o-dichlorobenzene (DCB)	1.14	490	1.958
chloroform (CH)	2.53	478	1.944
o-dichlorobenzene:chloroform cosolvent (DCB:CH)	2.82	514	1.916

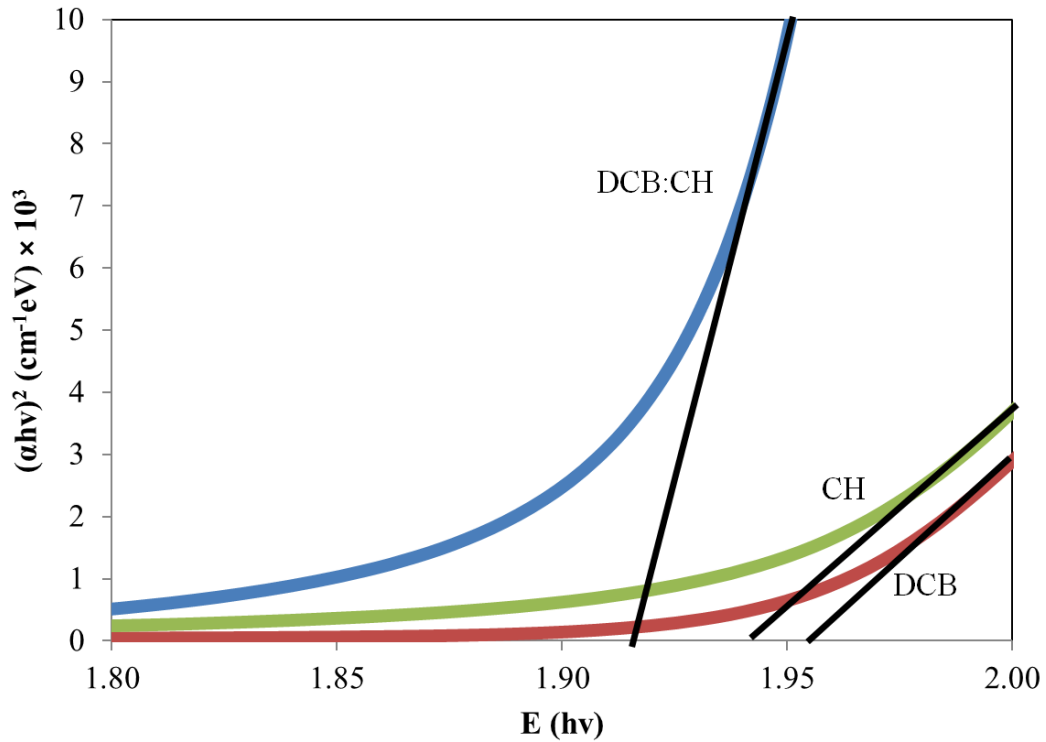


Figure 4.3.2: The plot of $(\alpha hv)^2$ vs hv of P3HT:PCBM blend films which were dissolved in pure DCB solvent, pure CH solvent and DCB:CH cosolvent.

By applying equation 4.1 (see part 4.1.1), a graph of $(\alpha hv)^2$ versus hv can be plotted to estimate the optical energy gap of the samples as shown in Figure 4.3.3. Extrapolating the straight line to $hv = 0$ will give the value of the optical energy gap for the DCB, CH, and DCB:CH samples and it was found that the optical energy gap is 1.958 eV, 1.944 eV, and 1.916 eV, respectively.

Table 4.3.1 shows the influence of different solvents on the values of maximum absorption coefficient, absorption peak and optical energy gap. By mixing the chloroform and dicholobenzene to form DCB:CH co-solvent, then the produced P3HT:PCBM film from such co-solvent has reduced the optical energy gap by 2% as compared to the film prepared from pure chloroform. Besides, the peak wavelength has been red-shifted by changing the film from the pure solvents to the co-solvent. The reduction in optical energy gap and red-shift of absorption will significantly enhance the photovoltaic properties of the device.

4.3.2 X-ray Diffraction Spectra

Figure 4.3.4 shows the XRD spectra of P3HT:PCBM blend films prepared in pure DCB, pure CH and DCB:CH co-solvent. In the spin-coated P3HT:PCBM blend films, only the first peak at $2\theta \approx 5.4^\circ$ in the diffractogram, corresponding to the first-order reflection, is normally observed (Alemany et al., 2008; Erb, et al., 2005; Vanlaeke, Swinnen, et al., 2006; Vanlaeke, Vanhoyland, et al., 2006; Zhokhavets, et al., 2006). This peak is attributed to the partial crystallinity of the P3HT crystallites which are dispersed in the amorphous regions of PCBM matrix.

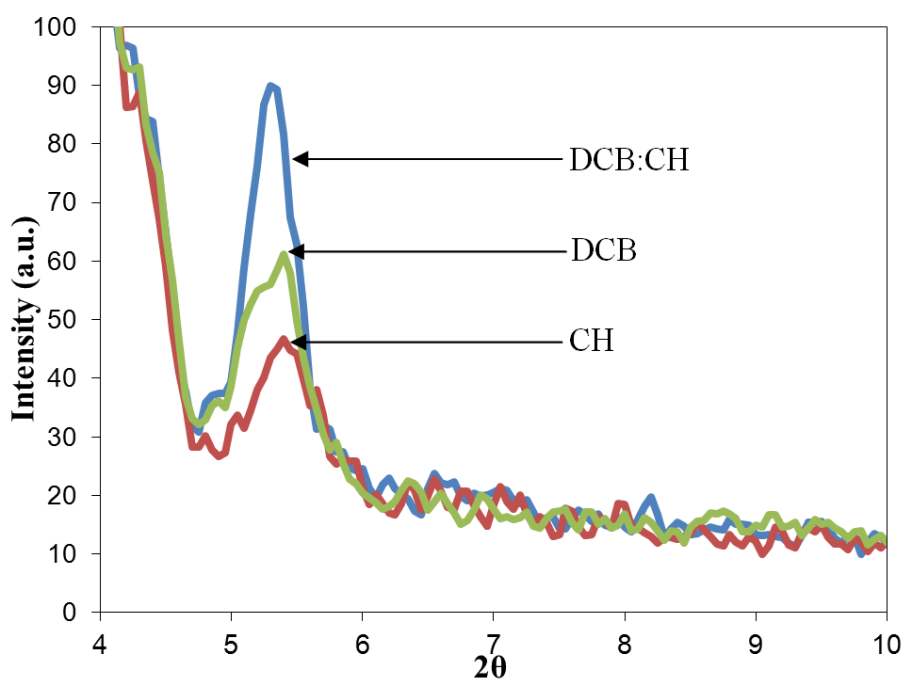


Figure 4.3.3: X-ray Diffraction of P3HT:PCBM blend films prepared in pure DCB, CH and DCB:CH co-solvent.

Table 4.3.2: Summary of the interplanar distance and the crystalline thickness for the DCB solvent, CH solvent and DCB:CH cosolvent.

Solvent Type	CH	DCB	DCB:CH
2θ (°)	5.40	5.35	5.30
FWHM (B) (rad)	0.00873	0.00873	0.00698
Interplanar Distance (d-spacing) (nm)	1.64	1.65	1.67
Crystalline Thickness (nm)	16.60	16.62	20.79
AFM surface roughness rms (nm)	12.6	11.0	14.3

The XRD result indicates that the film prepared from DCB:CH co-solvent shows the highest value of intensity peak and the smallest FWHM value representing having the highest degree of crystallization and the largest grain size of P3HT domain. Again, by using Scherrer's equation, the thickness of the crystallite was calculated. The thickness of crystallite size for the sample using co-solvent was increased with the value 20.79 nm compared with the sample using a single solvent of DCB and CH with the value of 16.62 nm and 16.60 nm respectively. The interplanar distance (d-spacing) is also slightly increases for the co-solvent fabricated film compare to the single solvent fabricated film with the value of 1.67 nm compare to 1.65 nm for DCB and 1.64 nm for CH. These results were in a good agreement with the absorption spectra of the samples. The crystallinity and the ordering of the polymer can be improved using DCB:CH co-solvent rather than using merely pure DCB or CH solvent. Table 4.3.2 summarizes of the interplanar distance and the crystalline thickness for all three samples.

4.3.3 Atomic Force Microscopy

Figure 4.3.5 shows the atomic force microscopy (AFM) images in three dimensional (3D) for P3HT:PCBM blend films dissolved in pure DCB solvent, CH solvent and DCB:CH co-solvent. The root-mean-square (rms) roughness of these layers is 11.0 nm, 12.6 nm and 14.3 nm respectively. This indicates that the film dissolved in DCB:CH co-solvent has a coarser surface morphology compared to that of pure DCB and CH since it shows a higher rms roughness value. This may attribute to the better solubility of the mixture components of DCB:CH co-solvent that lead to the increase in phase separation upon the films.

It is noted that the solvent evaporation rates can influence the surface morphology of the polymer films as summarized in Table 4.3.2. Although pure CH can aid to improve the surface affinity, but it possesses a higher solvent evaporation rate than the pure DCB solvent, and hence evaporate faster than the DCB, leading to a reduction in interface area of the blend films. However, by mixing both solvents together, the resulting solvent evaporation rate of the co-solvent can thus be modified. Besides, the solvating power (the ability to form strong secondary bonds between solvent and solute molecules) may also significantly affect the morphology of the films, since a good solvent can lead to a more extended polymer chain in solid state.

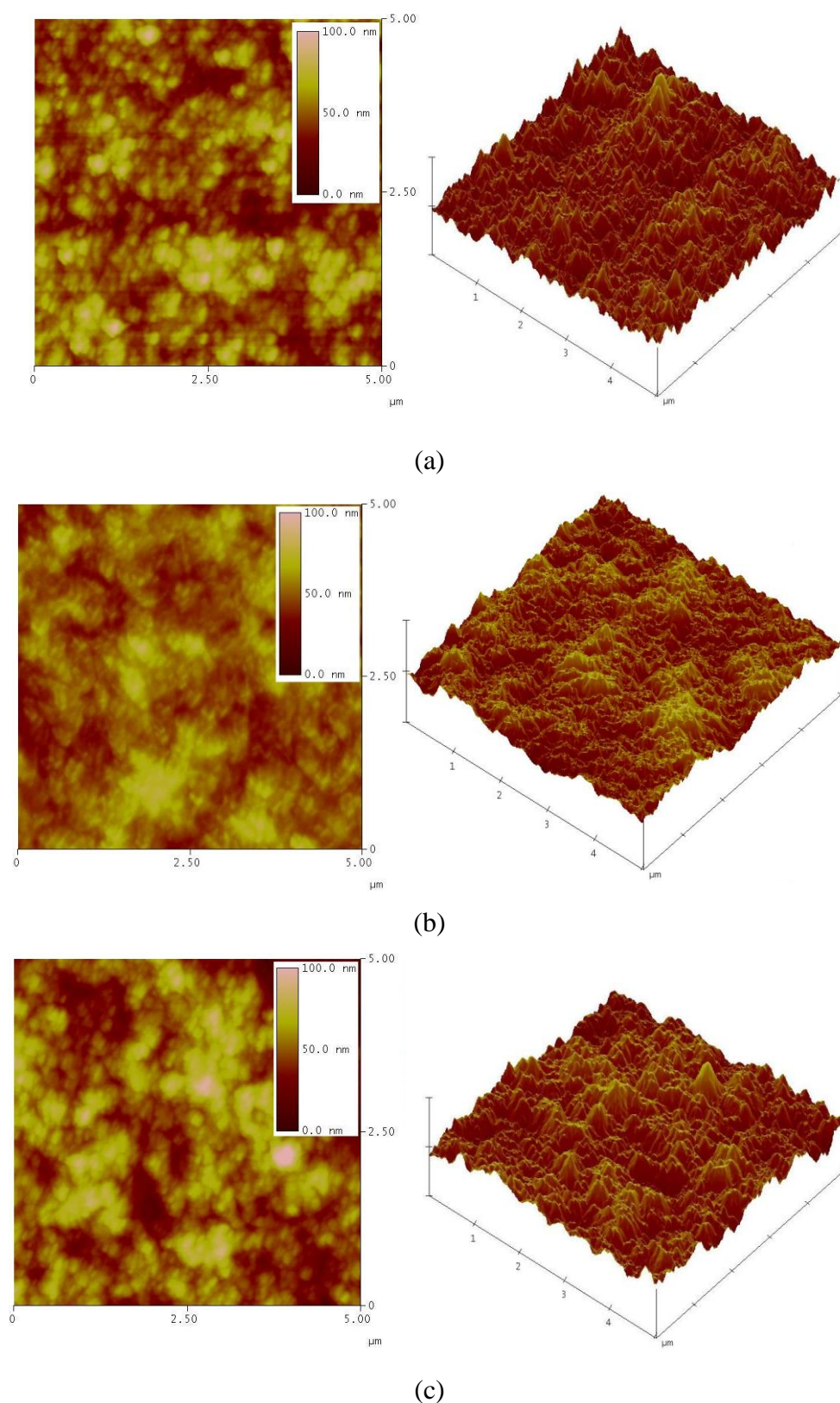


Figure 4.3.4: 2D and 3D atomic force microscopy images of P3HT:PCBM blend films dissolved in (a) pure DCB solvent, (b) CH solvent, and (c) DCB:CH cosolvent

The mixture of both DCB and CH produces a higher solvating power and yield a better blending of P3HT and PCBM. And thus, it results in an increase of phase separation on the film, leading to the formation of continuous pathways for electron and hole carriers and increases the interface area enhancing the exciton dissociation (Kwong, et al., 2004).

4.3.4 J-V Characteristic

Figure 4.3.5 shows the current density-voltage (J-V) characteristic curves and device parameters of the short-circuit current density (J_{sc}), open-circuit voltage (V_{oc}), fill factor (FF) and power conversion efficiency (PCE) values of the solar cells that corresponding to the blend films prepared from pure DCB, CH, and DCB:CH co-solvent are depicted in Table 4.1.3. The J_{sc} of the device prepared in pure DCB is 0.56 mA/cm², the V_{oc} is 0.26 V, and the FF is 0.38. These values contribute to a PCE of 0.06%. The device in DCB:CH co-solvent performs a better J_{sc} that increases up to 0.88 mA/cm² whereas the FF is increased to 0.78, and thus the corresponding PCE now equals to 0.25%. However, the worst performance is shown for the device in pure CH solvent, with a FF of 0.10 and PCE of 0.03%.

The observed improvement in the electrical properties of the P3HT:PCBM solar cell devices of the films prepared from co-solvent is attributed to the favorable change upon the enhanced crystallinity and surface morphology of the P3HT:PCBM blend thin films that may due to the better solubility in the mixture solvent as discussed above. Kawano et al. (Kawano, et al., 2009) also reported the similar result for the films prepared from pure DCB and DCB:CH co-solvent. It is accepted that the J_{sc} depends on the absorption properties of the films and their charge carrier transport. On the other hand, the open-circuit voltage, V_{oc} can be approximated by the difference in the

electrodes' work function or by the difference in the Highest Occupied Molecular Orbital (HOMO) of the donor and the Lowest Unoccupied Molecular Orbital (LUMO) of the acceptor (Muhammad, et al., 2011). As a result of better light absorption for the film dissolve in co-solvent from previous section, the value of J_{sc} is increasing. A better surface morphology also contribute to the increment of the J_{sc} as a result of film deposited using co-solvent since the percolation path of the exciton was formed which result in better transport carrier in the photovoltaic device.

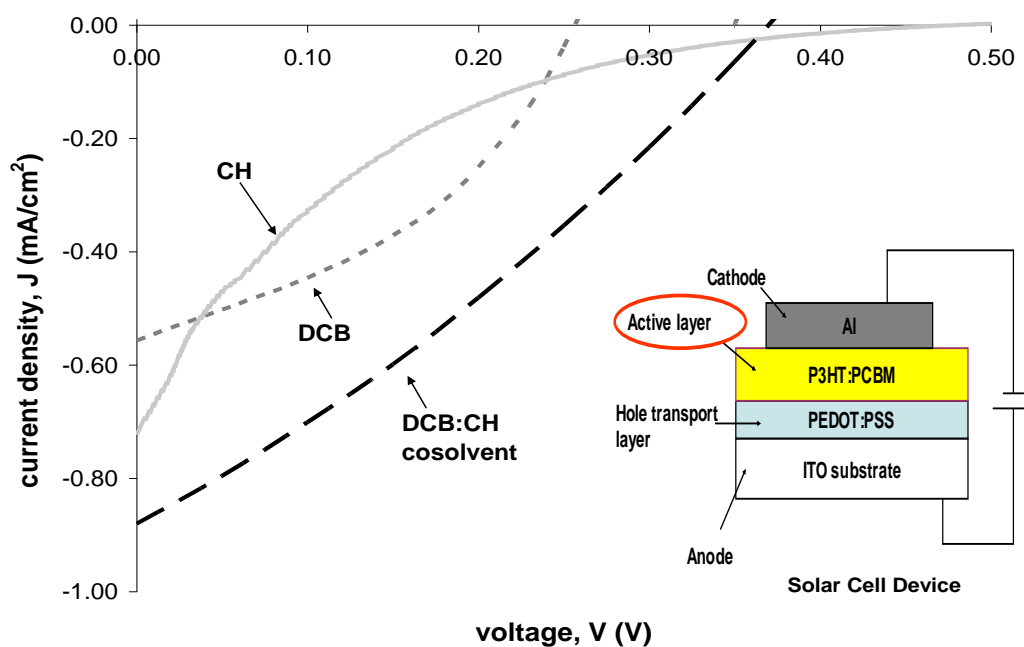


Figure 4.3.5: J-V plots for P3HT:PCBM solar cells prepared in DCB, CH and cosolvent. The inset shows the structure of ITO/PEDOT:PSS/P3HT:PCBM/Al solar cell device.

Table 4.3.3: The comparison of device characteristic parameters for P3HT:PCBM solar cells with active layers prepared in pure DCB, CH and DCB:CH cosolvent.

Solvent Type	DCB	CH	DCB:CH
V_{oc} (V)	0.26	0.48	0.37
J_{sc} (mA/cm ²)	0.56	0.72	0.88
V_{max} (V)	0.15	0.12	0.20
J_{max} (mA/cm ²)	0.37	0.033	1.03
FF	0.38	0.10	0.78
PCE (%)	0.06	0.03	0.25

4.3.5 Summary

As a summary, thermal annealing process on the PCBM blend films at 75 °C, 100 °C, 125 °C and 150 °C. This study shows that the optical, morphological and electrical properties of P3HT:PCBM solar cells can be significantly affected by the types of solvents. The phase separation of the P3HT:PCBM thin film is strongly influenced by the solubility of the mixture components of the chloroform-dichlorobenzene DCB:CH cosolvent. A mixture of solvent DCB:CH yields better solubility than the pure single solvent. Thus, a good solvent for P3HT:PCBM blend films with a lower solvent evaporation rate may favor better mixing of the compounds that result in improved the absorption coefficient, increased crystallite size of the films themselves, and consequently enhance the performances of the solar cell devices based on photoactive polymeric thin films.

Chapter Five

CONCLUSION

Conclusion

This research has been focusing on the properties of P3HT:PCBM mixture thin film. Three factors have been investigated to recognize how the material behaves in certain condition.

The preparation of the sample is done in a few stages. Starting with mixing the two materials with a solvent, the solution were stirred for more than 24 hours to make sure that the solution were properly mix. Spin coating method was use to fabricate the thin layer of the sample. Depending on the concentration and the speed of the spin coater, the desirable thickness of the sample was obtained.

In the first part of this study, the influence of annealing temperature was performed on the optical, structural and morphological properties of the P3HT:PCBM thin films. The P3HT:PCBM thin film has a range of absorption that occurs at both B-band and Q-band, ranging from 308 nm to 356 nm and 386 nm to 398 nm respectively. By thermal treating the sample from 75 °C to 150 °C, it was found that the absorption intensity of the sample has increased and red shifted to the higher wavelength. This is the earliest indication that by thermal treating the sample, there is a formation of PCBM cluster in the film and the crystallites of the sample were improved by re-arrangement of the polymer chain. Calculation of the optical energy gap has shown that the optical energy gap has increased as the temperature applied to the sample increased. XRD studies were performed to further study the crystallization of the samples, and peaks at approximately 2θ of 5.4° was found for P3HT:PCBM samples. It was also found that the diffraction peak for the P3HT sample shifted to a higher 2θ angle after PCBM were introduce to the sample. By thermal treating the sample, the crystallites of the sample

were restored. This also means annealing has increased the interplanar distance (d-spacing) of the thin film sample. This finding support the result obtained from the absorption spectroscopy measurement. The optimum annealing temperature was found to be at 125 °C to produce the biggest absorption range as well as the largest crystallite size of P3HT:PCBM thin film. With these findings, it can be concluded that annealing can improve the solar cells performance as it can increase the crystalline domains in the active layer.

In the second part of the study, the effect of slow film formation of P3HT:PCBM blend film has been investigated. The optimum temperature of 125 °C was used for the preparation of the fast grown and slow grown film fabrication process. From optical absorption, Raman spectroscopy, X-ray diffraction, and Atomic Force Microscopy measurement it has been revealed that the morphology and optical properties of the sample have improved upon the fast grown process of thermal annealing. Furthermore, a better polymer ordering and higher crystallinity have been obtained via the slow grown process. It has been demonstrated that slow grown lead to a remarkable increase in the photovoltaic effect. Slowing the film formation in the sample leads to a better structural and ordering in the P3HT:PCBM phase. This creates a more crystallite sample that provides a better transport for hole through a more improved ordering. The improvement of the short-circuit current and open circuit voltage obtained from the photovoltaic characteristic is due to the enhancement in the semi-crystallite size of the polymer blend. Slow grown has proven to be a successful way to fabricate a good high efficiencies solar cell. Thus it can be said that the slow grown technique of the polymer film can be used as another alternative to improve the formation in the sample and the device performance other than using thermal annealing process. This is useful especially for a temperature sensitive substrate and materials.

In the final part of this research work, the influence of solvent used in the preparation of the polymer thin film, was investigated on the absorption coefficient, optical energy gap, phase separation, crystallinity as well as photovoltaic properties. The results show that the phase separation of the P3HT:PCBM thin film is strongly influenced by the solubility of the mixture component of the DCB:CH co-solvent. A mixture of solvent DCB:CH yields a better solubility than the pure single solvent of DCB or chloroform. The DCB:CH co-solvent has a lower solvent evaporation rate may give better mixing of the polymer, producing a good morphological behavior with enhanced mobility (due to higher crystallinity). Consequently enhance the performances of the solar cell devices based on photoactive polymeric thin films.

In this research work, all preparation of the thin films as well as the fabrication of the device, were performed under ambient air. The glove-box facility was not available during this study, thus all the fabricated devices were easily oxidized with low current. Hence, more research can be carried out in order to further improve and to understand the full performance of this material combination.

Here are some suggestions for future work:

- Studies the effect of P3HT:PCBM compositions (weight ratios), using the optimum temperature of 125 °C and the chloroform:dichlorobenzene cosolvent in the film preparation.
- Structural study can be further investigated using a Small-Angle X-Ray Diffraction Technique.
- The microscopic properties of the P3HT:PCBM blend films may be visualized by utilizing Field Effect Scanning Electron Microscopy (FESEM).
- Fabrication of the devices in a glove-box to obtain the encapsulated organic P3HT:PCBM solar cells and make comparison to the un-encapsulated device.

BIBLIOGRAPHY

Bibliography

- Al-Ibrahim, M., Roth, H. K., Zhokhavets, U., Gobsch, G., & Sensfuss, S. (2005). Flexible large area polymer solar cells based on poly(3-hexylthiophene)/fullerene. *Solar Energy Materials and Solar Cells*, 85(1), 13-20.
- Aleman, J. A., Frystyk, J., Tuckow, A. P., Spiering, B. A., Hatfield, D. L., Staab, J. S., Chen, J. W., Flyvbjerg, A., Maresh, C. M., Kraemer, W. J., & Nindl, B. C. (2008). Effects Of Resistance, Aerobic And Combined Exercise Training On Immunoreactive Vs. Bioassayable IGF-I. *Medicine and Science in Sports and Exercise*, 40(5), S105-S105.
- Atomic force microscopy. (2012) Retrieved February 15, 2012, from http://en.wikipedia.org/w/index.php?title=Atomic_force_microscopy&oldid=497369954
- Brabec, C. J., Sariciftci, N. S., & Hummelen, J. C. (2001). Plastic Solar Cells. *Advanced Functional Materials*, 11(1), 15-26.
- Brabec, C. J., Shaheen, S. E., Winder, C., Sariciftci, N. S., & Denk, P. (2002). Effect of LiF/metal electrodes on the performance of plastic solar cells. *Applied Physics Letters*, 80(7), 1288-1290.
- Breeze, A. J., Salomon, A., Ginley, D. S., Gregg, B. A., Tillmann, H., & Horhold, H. H. (2002). Polymer---perylene diimide heterojunction solar cells. *Applied Physics Letters*, 81(16), 3085-3087.
- Brown, P. J., Thomas, D. S., Kohler, A., Wilson, J. S., Kim, J. S., Ramsdale, C. M., Sirringhaus, H., & Friend, R. H. (2003). Effect of interchain interactions on the absorption and emission of poly (3-hexylthiophene). *Physical Review B*, 67(6), 64203-64203.
- Brown, T. M., Kim, J. S., Friend, R. H., Cacialli, F., Daik, R., & Feast, W. J. (1999). Built-in field electroabsorption spectroscopy of polymer light-emitting diodes incorporating a doped poly(3,4-ethylene dioxythiophene) hole injection layer. *Applied Physics Letters*, 75(12), 1679-1681.
- Campbell, C. J., & Laherrere, J. H. . (1998). The End of Cheap Oil. *Scientific American March*.
- Cao, Y., Andreatta, A., Heeger, A. J., & Smith, P. (1989). Influence of chemical polymerization conditions on the properties of polyaniline. *Polymer*, 30(12), 2305-2311.

- Chang, J.-F., Sun, B., Breiby, D. W., Nielsen, M. M., Sölling, T. I., Giles, M., McCulloch, I., & Sringhaus, H. (2004). Enhanced Mobility of Poly(3-hexylthiophene) Transistors by Spin-Coating from High-Boiling-Point Solvents. *Chemistry of Materials*, *16*(23), 4772-4776.
- Chen, L. M., Hong, Z., Li, G., & Yang, Y. (2009). Recent progress in polymer solar cells: manipulation of polymer: fullerene morphology and the formation of efficient inverted polymer solar cells. *Advanced Materials*, *21*(14-15), 1434-1449.
- Chen, T. A., Wu, X., & Rieke, R. D. (1995). Regiocontrolled synthesis of poly (3-alkylthiophenes) mediated by Rieke zinc: their characterization and solid-state properties. *Journal of the American Chemical Society*, *117*(1), 233-244.
- Chirvase, D., Parisi, J., Hummelen, J., & Dyakonov, V. (2004). Influence of nanomorphology on the photovoltaic action of polymer–fullerene composites. *Nanotechnology*, *15*, 1317.
- Coakley, K. M., & McGehee, M. D. (2004). Conjugated Polymer Photovoltaic Cells. *Chemistry of Materials*, *16*(23), 4533-4542.
- Cojan, C., Agrawal, G. P., & Flytzanis, C. (1977). Optical properties of one-dimensional semiconductors and conjugated polymers. *Physical Review B*, *15*(2), 909-925.
- Dridi, C., Benzarti-Ghédira, M., Vocanson, F., Ben Chaabane, R., Davenas, J., & Ben Ouada, H. (2009). Optical and electrical properties of semi-conducting calix [5, 9] arene thin films with potential applications in organic electronics. *Semiconductor Science and Technology*, *24*, 105007.
- Dyakonov, V. (2002). The polymer–fullerene interpenetrating network: one route to a solar cell approach. *Physica E: Low-dimensional Systems and Nanostructures*, *14*(1–2), 53-60.
- El-Nahass, M. M., El-Gohary, Z., & Soliman, H. S. (2003). Structural and optical studies of thermally evaporated CoPc thin films. *Optics & Laser Technology*, *35*(7), 523-531.
- Erb, T., Zhokhavets, U., Gobsch, G., Raleva, S., Stühn, B., Schilinsky, P., Waldauf, C., & Brabec, C. J. (2005). Correlation between structural and optical properties of composite polymer/fullerene films for organic solar cells. *Advanced Functional Materials*, *15*(7), 1193-1196.
- Ge, N. (2009). An overview on P3HT : PCBM , the most efficient organic solar cell material so far. *Solid State Physics*, (Fig 1), 1-11.

- Gebeyehu, D., Maennig, B., Drechsel, J., Leo, K., & Pfeiffer, M. (2003). Bulk-heterojunction photovoltaic devices based on donor-acceptor organic small molecule blends. *Solar Energy Materials and Solar Cells*, 79(1), 81-92.
- Gebeyehu, D., Pfeiffer, M., Maennig, B., Drechsel, J., Werner, A., & Leo, K. (2004). Highly efficient p-i-n type organic photovoltaic devices. *Thin Solid Films*, 451-452(0), 29-32.
- Ghosh, A. K., & Feng, T. (1978). Merocyanine organic solar cells. *Journal of Applied Physics*, 49(12), 5982-5989.
- Granstrom, M., Petritsch, K., Arias, A. C., Lux, A., Andersson, M. R., & Friend, R. H. (1998). Laminated fabrication of polymeric photovoltaic diodes. *Nature*, 395(6699), 257-260.
- Greczynski, C., Fahlman, M., Salaneck W.R. (1996). *J. Chem. Phys.*, 69, 599.
- Green, M. A., Emery, K., Hishikawa, Y., Warta, W., & Dunlop, E. D. (2012). Solar cell efficiency tables (version 39). *Progress in Photovoltaics: Research and Applications*, 20(1), 12-20.
- Guo, T. F., Wen, T. C., L'vovich Pakhomov, G., Chin, X. G., Liou, S. H., Yeh, P. H., & Yang, C. H. (2008). Effects of film treatment on the performance of poly(3-hexylthiophene)/soluble fullerene-based organic solar cells. *Thin Solid Films*, 516(10), 3138-3142.
- Halls, J. J. M., & Friend, R. H. (1997). The photovoltaic effect in a poly(p-phenylenevinylene)/perylene heterojunction. *Synthetic Metals*, 85(1-3), 1307-1308.
- Halls, J. J. M., Pichler, K., Friend, R. H., Moratti, S. C., & Holmes, A. B. (1996). Exciton diffusion and dissociation in a poly(p-phenylenevinylene)/C₆₀ heterojunction photovoltaic cell. *Applied Physics Letters*, 68(22), 3120-3122.
- Hatfield, C. B. (1997). Oil back on the global agenda. *Nature*, 387(6629), 121.
- Hauch, J. A., Schilinsky, P., Choulis, S. A., Childers, R., Biele, M., & Brabec, C. J. (2008). Flexible organic P3HT:PCBM bulk-heterojunction modules with more than 1 year outdoor lifetime. *Solar Energy Materials and Solar Cells*, 92(7), 727-731.
- Heller, C., Leising, G., Godon, C., Lefrant, S., Fischer, W., & Stelzer, F. (1995). Raman excitation profiles of conjugated segments in solution. *Physical Review B*, 51(13), 8107.

- Hiramoto, M., Fujiwara, H., & Yokoyama, M. (1991). Three-layered organic solar cell with a photoactive interlayer of codeposited pigments. *Applied Physics Letters*, 58(10), 1062-1064.
- Hiramoto, M., Fukusumi, H., & Yokoyama, M. (1992). Organic solar cell based on multistep charge separation system. *Applied Physics Letters*, 61(21), 2580-2582.
- Hiramoto, M., Kishigami, Y., & Yokohama, M. (1990). *Chem. Lett.*, 19 119.
- Horowitz, G. (1998). Organic Field-Effect Transistors. *Advanced Materials*, 10(5), 365-377.
- Hung, L. S., Tang, C. W., & Mason, M. G. (1997). Enhanced electron injection in organic electroluminescence devices using an Al/LiF electrode. *Applied Physics Letters*, 70(2), 152-154.
- Jiang, X. M., Österbacka, R., Korovyanko, O., An, C. P., Horovitz, B., Janssen, R. A. J., & Vardeny, Z. V. (2002). Spectroscopic Studies of Photoexcitations in Regioregular and Regiorandom Polythiophene Films. *Advanced Functional Materials*, 12(9), 587-597.
- Jin, S.-H., Vijaya Kumar Naidu, B., Jeon, H.-S., Park, S.-M., Park, J.-S., Chul Kim, S., Wook Lee, J., & Gal, Y.-S. (2007). Optimization of process parameters for high-efficiency polymer photovoltaic devices based on P3HT:PCBM system. *Solar Energy Materials and Solar Cells*, 91(13), 1187-1193.
- Jönsson, S. K. M., Birgersson, J., Crispin, X., Greczynski, G., Osikowicz, W., Denier van der Gon, A. W., Salaneck, W. R., & Fahlman, M. (2003). The effects of solvents on the morphology and sheet resistance in poly(3,4-ethylenedioxythiophene)-polystyrenesulfonic acid (PEDOT-PSS) films. *Synthetic Metals*, 139(1), 1-10.
- Kalinowski, J. (1999). Electroluminescence in Organics. *Journal of Physics D: Applied Physics*, 32 179-250.
- Katz, E. A., Faiman, D., Tuladhar, S. M., Kroon, J. M., Wienk, M. M., Fromherz, T., Padinger, F., Brabec, C. J., & Sariciftci, N. S. (2001). Temperature dependence for the photovoltaic device parameters of polymer-fullerene solar cells under operating conditions. *Journal of Applied Physics*, 90(10), 5343-5350.
- Kawano, K., Sakai, J., Yahiro, M., & Adachi, C. (2009). Effect of solvent on fabrication of active layers in organic solar cells based on poly (3-hexylthiophene) and fullerene derivatives. *Solar Energy Materials and Solar Cells*, 93(4), 514-518.

- Kim, H., So, W., & Moon, S. (2006). Effect of thermal annealing on the performance of P3HT/PCBM polymer photovoltaic cells. *Journal Of The Korean Physical Society*, 48(3), 441-445.
- Kim, J. S., Granstrom, M., Friend, R. H., Johansson, N., Salaneck, W. R., Daik, R., Feast, W. J., & Cacialli, F. (1998). Indium--tin oxide treatments for single- and double-layer polymeric light-emitting diodes: The relation between the anode physical, chemical, and morphological properties and the device performance. *Journal of Applied Physics*, 84(12), 6859-6870.
- Kim, J. Y., Jung, J. H., Lee, D. E., & Joo, J. (2002). Enhancement of electrical conductivity of poly(3,4-ethylenedioxythiophene)/poly(4-styrenesulfonate) by a change of solvents. *Synthetic Metals*, 126(2-3), 311-316.
- Kittel, C. (1972). *Introduction a la physique de l'etat solide*. Bordas, Paris.
- Klein, M., & Cardona, M. (1975). Light scattering in solids. *Topics in Applied Physics*, 8, 147.
- Klimov, E., Li, W., Yang, X., Hoffmann, G., & Loos, J. (2006). Scanning near-field and confocal Raman microscopic investigation of P3HT-PCBM systems for solar cell applications. *Macromolecules*, 39(13), 4493-4496.
- Kwong, C., Djurišić, A., Chui, P., Cheng, K., & Chan, W. (2004). Influence of solvent on film morphology and device performance of poly (3-hexylthiophene): TiO₂ nanocomposite solar cells. *Chemical Physics Letters*, 384(4), 372-375.
- Li, G., Yao, Y., Yang, H., Shrotriya, V., Yang, G., & Yang, Y. (2007). "Solvent Annealing" Effect in Polymer Solar Cells Based on Poly (3-hexylthiophene) and Methanofullerenes. *Advanced Functional Materials*, 17(10), 1636-1644.
- Louarn, G., Trznadel, M., Buisson, J. P., Laska, J., Pron, A., Lapkowski, M., & Lefrant, S. (1996). Raman Spectroscopic Studies of Regioregular Poly(3-alkylthiophenes). *The Journal of Physical Chemistry*, 100(30), 12532-12539.
- Mailis, S., Boutsikaris, L., Vainos, N. A., Xirouhaki, C., Vasiliou, G., Garawal, N., Kiriakidis, G., & Fritzsche, H. (1996). Holographic recording in indium-oxide (In₂O₃) and indium-tin-oxide (In₂O₃: Sn) thin films. *Applied Physics Letters*, 69(17), 2459-2461.
- Mark, J. A. (1996). *Physical properties of polymers handbook*. New York: American Institute of Physics.

- Marks, R. N., Halls, J. J. M., Bradley, D. D. C., Friend, R. H., & Holmes, A. B. (1994). The photovoltaic response in poly(p-phenylene vinylene) thin-film devices. *Journal of Physics: Condensed Matter*, 6(7), 1379.
- Mehta, A. (2012) Ultraviolet-Visible (UV-Vis) Spectroscopy – Derivation of Beer-Lambert Law Retrieved February 15, 2012, from <http://pharmaxchange.info/press/2012/04/ultraviolet-visible-uv-vis-spectroscopy-%e2%80%93-derivation-of-beer-lambert-law/>
- Mihailetchi, V. D., Xie, H., de Boer, B., Koster, L. J. A., & Blom, P. W. M. (2006). Charge transport and photocurrent generation in poly (3-hexylthiophene): methanofullerene bulk-heterojunction solar cells. *Advanced Functional Materials*, 16(5), 699-708.
- Moss, S. C. (Ed.). (2002). *Organic Optoelectronic Materials, Processing and Devices* (Vol. 708): Materials Research Society
- Muhammad, F. F., Abdul Hapip, A. I., & Sulaiman, K. (2010). Study of optoelectronic energy bands and molecular energy levels of tris (8-hydroxyquinolate) gallium and aluminum organometallic materials from their spectroscopic and electrochemical analysis. *Journal of Organometallic Chemistry*, 695(23), 2526-2531.
- Muhammad, F. F., & Sulaiman, K. (2011). Photovoltaic Performance of Organic Solar Cells Based on DH6T/PCBM Thin Film Active Layers. *Thin Solid Films*, 519 5230- 5233.
- Muhammad, F. F., & Sulaiman, K. (2011). Effects of thermal annealing on the optical, spectroscopic, and structural properties of tris (8-hydroxyquinolate) gallium films grown on quartz substrates. . *Materials Chemistry and Physics*, 129 (3), 1152-1158.
- Nalwa, H. S. (1996). *Handbook of organic conductive molecules and polymers*. New York: John Wiley & Sons.
- Nunzi, J.-M. (2002). Organic photovoltaic materials and devices. *Comptes Rendus Physique*, 3(4), 523-542.
- Petritsch, K. (2000). Organic solar cell architectures. *Cambridge and Graz*.
- Pettersson, L. A. A., Roman, L. S., & Inganas, O. (1999). Modeling photocurrent action spectra of photovoltaic devices based on organic thin films. *Journal of Applied Physics*, 86(1), 487-496.

- Petty, M. C. (2000). Organic Thin-Film Deposition Techniques. In T. H. Richardson (Ed.), *Functional organic and polymeric materials: molecular functionality macroscopic reality*: Wiley.
- Petty, M. C., Bryce, M. R., & Bloor, D. (1995). *Introduction to Molecular Electronics*. London: Edward Arnold.
- Peumans, P., & Forrest, S. R. (2001). Very-high-efficiency double-heterostructure copper phthalocyanine/C₆₀ photovoltaic cells. *Applied Physics Letters*, 79(1), 126-128.
- Peumans, P., Yakimov, A., & Forrest, S. R. (2003). Small molecular weight organic thin-film photodetectors and solar cells. *Journal of Applied Physics*, 93(7), 3693-3723.
- Pissadakis, S., Mailis, S., Reekie, L., Wilkinson, J.S., Eason, R.W., Vainos, N.A., Moschovis, K., Kiriakdikis, G. (1999). *Appl. Phys. A*, 69, 333.
- Roman, L. S., Mammo, W., Pettersson, L. A. A., Andersson, M. R., & Inganäs, O. (1998). High Quantum Efficiency Polythiophene. *Advanced Materials*, 10(10), 774-777.
- Rostalski, J., & Meissner, D. (2000). Photocurrent Spectroscopy: A New Method for the Investigation of Charge Carrier Generation and Transport Mechanisms in Organic p/n Junction Solar Cells *Sol. Energy Mater. Sol. Cells*, 63, 37.
- Roth, S., & Carroll, D. (2004). *One-Dimensional Metals: Conjugated Polymers, Organic Crystals, Carbon Nanotubes* (2nd Ed ed.). Weinheim, New York: WileyVCH.
- Sariciftci, N. S., Braun, D., Zhang, C., Srdanov, V. I., Heeger, A. J., Stucky, G., & Wudl, F. (1993). Semiconducting polymer-buckminsterfullerene heterojunctions: Diodes, photodiodes, and photovoltaic cells. *Applied Physics Letters*, 62(6), 585-587.
- Schilinsky, P., Waldauf, C., & Brabec, C. J. (2002). Recombination and loss analysis in polythiophene based bulk heterojunction photodetectors. *Applied Physics Letters*, 81(20), 3885-3887.
- Schlatmann, A. R., Floet, D. W., Hilberer, A., Garten, F., Smulders, P. J. M., Klapwijk, T. M., & Hadziioannou, G. (1996). Indium contamination from the indium--tin-oxide electrode in polymer light-emitting diodes. *Applied Physics Letters*, 69(12), 1764-1766.

- Scott, J. C., Kaufman, J. H., Brock, P. J., DiPietro, R., Salem, J., & Goitia, J. A. (1996). Degradation and failure of MEH-PPV light-emitting diodes. *Journal of Applied Physics*, 79(5), 2745-2751.
- Shockley, W., & Queisser, H. J. (1961). Detailed Balance Limit of Efficiency of p-n Junction Solar Cells. *Journal of Applied Physics*, 32(3), 510-519.
- Shrotriya, V., Ouyang, J., Tseng, R. J., Li, G., & Yang, Y. (2005). Absorption spectra modification in poly (3-hexylthiophene): methanofullerene blend thin films. *Chemical Physics Letters*, 411(1), 138-143.
- Sirringhaus, H., Brown, P. J., Friend, R. H., Nielsen, M. M., Bechgaard, K., Langeveld-Voss, B. M. W., Spiering, A. J. H., Janssen, R. A. J., Meijer, E. W., Herwig, P., & de Leeuw, D. M. (1999). Two-dimensional charge transport in self-organized, high-mobility conjugated polymers. *Nature*, 401(6754), 685-688.
- Sirringhaus, H., Tessler, N., & Friend, R. H. (1998). Integrated Optoelectronic Devices Based on Conjugated Polymers. *Science*, 280(5370), 1741-1744.
- Skompska, M. (2010). Hybrid conjugated polymer/semiconductor photovoltaic cells. *Synthetic Metals*, 160(1-2), 1-15.
- Skotheim, T. J., Elsenbaumer, R.L., Reynolds, J.R. (1998). *Handbook of conducting polymers*. New York: Dekker.
- Spanggaard, H., & Krebs, F. C. (2004). A brief history of the development of organic and polymeric photovoltaics. *Solar Energy Materials and Solar Cells*, 83(2-3), 125-146.
- Su, W. P., Schrieffer, J. R., & Heeger, A. J. (1979). Solitons in Polyacetylene. *Physical Review Letters*, 42(25), 1698-1701.
- Sugiyama, K., Ishii, H., Ouchi, Y., Seki, K. (2003). *J. Appl. Phys.*, 87, 295.
- Sun, S., Fan, Z., Wang, Y., & Haliburton, J. (2005). Organic solar cell optimizations. *Journal of materials science*, 40(6), 1429-1443.
- Sze, S. M., Ng, K. K. (2007). *Physics of Semiconductor Devices*. New York: John Wiley & Sons.
- Tang, C. W. (1986). Two-layer organic photovoltaic cell. *Applied Physics Letters*, 48(2), 183-185.

- Tang, C. W., & Albrecht, A. C. (1975). Photovoltaic Effects of Metal-chlorophyll-a-metal Sandwich Cells. *J. Chem. Phys.*, 62, 2139.
- Tang, H., Li, F., & Shinar, J. (1997). Bright high efficiency blue organic light-emitting diodes with Al₂O₃/Al cathodes. *Applied Physics Letters*, 71(18), 2560-2562.
- Tauc, J. (1968). Optical properties and electronic structure of amorphous Ge and Si. *Materials Research Bulletin*, 3(1), 37-46.
- Vanlaeke, P., Swinnen, A., Haeldermans, I., Vanhoyland, G., Aernouts, T., Cheyns, D., Deibel, C., D'Haen, J., Heremans, P., Poortmans, J., & Manca, J. V. (2006). P3HT/PCBM bulk heterojunction solar cells: Relation between morphology and electro-optical characteristics. *Solar Energy Materials and Solar Cells*, 90(14), 2150-2158.
- Vanlaeke, P., Vanhoyland, G., Aernouts, T., Cheyns, D., Deibel, C., Manca, J., Heremans, P., & Poortmans, J. (2006). Polythiophene based bulk heterojunction solar cells: Morphology and its implications. *Thin Solid Films*, 511, 358-361.
- Wallace, G. G., Dastoor, P. C., & Officer, D. L. (2000). Conjugated Polymers: New materials for photovoltaics. *Chemical Innovation*, 30, 14-22.
- Wang, T.-L., Yang, C.-H., Shieh, Y.-T., Chen, Y.-C., Ho, T.-H., & Chen, C.-H. (2012). An extremely low bandgap donor-acceptor copolymer for panchromatic solar cells. *Solar Energy Materials and Solar Cells*.
- Warm global temperatures continue in 2011.* (2011). Retrieved from <http://www.metoffice.gov.uk/news/releases/archive/2011/2011-global-temperature>
- Wöhrle, D., & Meissner, D. (1991). Organic Solar Cells. *Advanced Materials*, 3(3), 129-138.
- Wu, C. C., Wu, C. I., Sturm, J. C., & Kahn, A. (1997). Surface modification of indium tin oxide by plasma treatment: An effective method to improve the efficiency, brightness, and reliability of organic light emitting devices. *Applied Physics Letters*, 70(11), 1348-1350.
- Xiaoyin, X., Heongkyu, J., & Eun-Cheol, L. (2010). Band gap enhancement by covalent interactions in P3HT/PCBM photovoltaic heterojunction. *Journal Of The Korean Physical Society*, 57(1).

- Xie, W., Sun, Y. Y., Zhang, S. B., & Northrup, J. E. (2011). Structure and sources of disorder in poly(3-hexylthiophene) crystals investigated by density functional calculations with van der Waals interactions. *Physical Review B*, 83(18), 184117.
- Xirochaki, C., Moschovis, K., Chatzitheodoridis, E., Kiriakidis, G., Morgen, P. (1998). *Appl. Phys. A*, 67 295.
- Xirouchaki, C., Kiriakidis, G., Pedersen, T. F., & Fritzsche, H. (1996). Photoreduction and oxidation of as-deposited microcrystalline indium oxide. *Journal of Applied Physics*, 79(12), 9349-9352.
- Yamanari, T., Taima, T., Hara, K., & Saito, K. (2006). Investigation of optimum conditions for high-efficiency organic thin-film solar cells based on polymer blends. *Journal of Photochemistry and Photobiology A: Chemistry*, 182(3), 269-272.
- Yang, X., Loos, J., Veenstra, S. C., Verhees, W. J. H., Wienk, M. M., Kroon, J. M., Michels, M. A. J., & Janssen, R. A. J. (2005). Nanoscale Morphology of High-Performance Polymer Solar Cells. *Nano Letters*, 5(4), 579-583.
- Yao, Y., Hou, J., Xu, Z., Li, G., & Yang, Y. (2008). Effects of solvent mixtures on the nanoscale phase separation in polymer solar cells. *Advanced Functional Materials*, 18(12), 1783-1789.
- Yohannes, T., Zhang, F., Svensson, M., Hummelen, J. C., Andersson, M. R., & Inganäs, O. (2004). Polyfluorene copolymer based bulk heterojunction solar cells. *Thin Solid Films*, 449(1-2), 152-157.
- You, J., Dou, L., Yoshimura, K., Kato, T., Ohya, K., Moriarty, T., Emery, K., Chen, C.-C., Gao, J., & Li, G. (2013). A polymer tandem solar cell with 10.6% power conversion efficiency. *Nature communications*, 4, 1446.
- Yu, G., Gao, J., Hummelen, J. C., Wudl, F., & Heeger, A. J. (1995). Polymer Photovoltaic Cells: Enhanced Efficiencies via a Network of Internal Donor-Acceptor Heterojunctions. *Science*, 270(5243), 1789-1791.
- Yu, G., Pakbaz, K., & Heeger, A. J. (1994). Semiconducting polymer diodes: Large size, low cost photodetectors with excellent visible-ultraviolet sensitivity. *Applied Physics Letters*, 64(25), 3422-3424.
- Zhokhavets, U., Erb, T., Hoppe, H., Gobsch, G., & Serdar Sariciftci, N. (2006). Effect of annealing of poly (3-hexylthiophene)/fullerene bulk heterojunction composites on structural and optical properties. *Thin Solid Films*, 496(2), 679-682.